Mechanisms of Colloid Transport and Retention within Single Saturated Fractures

Analyzing the effects of ionic strength, particle size and particle characteristics on the transport mechanisms of colloids in single, saturated dolomite fractures.

Graham Seggewiss, B.Eng.Mgt.

A Thesis

Submitted to the School of Graduate Studies

In Partial Fulfillment of the Requirements

For the Degree

Master of Applied Science

McMaster University

MASTER OF APPLIED SCIENCE (2013) McMaster University

(Civil Engineering) Hamilton Ontario

Title:	Analyzing the effects of ionic strength, particle size and particle characteristics on the transport of colloids in single, saturated dolomite fractures.
Author:	Graham Seggewiss (McMaster University)
Supervisor:	Dr. Sarah E. Dickson
Number of Pages:	xii, 80

Abstract

A series of experiments were carried out to gain a better understanding of the mechanisms governing the transport of biological and non-biological particles through single, saturated dolomite fractures at the laboratory scale. Fracture apertures and general roughness were characterized using hydraulic and conservative solute tracer experiments. Influent and effluent recirculation cells were constructed to facilitate all experiments. Exact influent and effluent concentrations were calculated by assuming each cell acted as a continuously stirred tank reactor (CSTR), and also by accounting for biological decay where applicable.

The effects of particle size, surface characteristics and ionic strength of carrying solution were all evaluated. Particulate material studied included MS2, *E. coli* and two distinct sizes of carboxylated microspheres. To elucidate the effect of ionic strength on particulate transport, the ionic strength of the carrying solution was altered during each particulate test. Conservative tracer experiments were carried out at specific discharges of 5, 15 and 30 m/day. All particulate experiments were completed at 15 m/day to facilitate comparisons.

Recovery of biological particulate material was found to be much less relative to the carboxylated microspheres, even though the energy profiles predicted similar interactions with the fracture surface. This suggests that the biological surface has a significant impact on retention within the fracture. Further, altering the ionic strength of the carrying solution did not spur significant elution of additional particulate material, regardless of surface characteristics. Therefore, it was determined that retention within the secondary energy minimum was negligible under these operating conditions.

With respect to carboxylated microspheres, increased retention was observed within the less variable fracture. This suggests that increased variability within a fracture results in increased eddying within the aperture field. This eddying effectively reduces the aperture region available for particle transport, lessening the particle/fracture interaction. Overall, while mean residence times were similar, recovery of biological particles was poorly replicated by microspheres.

Acknowledgements

Firstly, I would like to thank Dr. Sarah Dickson for her guidance and supervision throughout this Masters degree. While the path was not always obvious to me, her kind support and expertise helped ensure I found my way. She was always eager to help and available for moral and intellectual support. She cared not only about fractured rock, but also about mental well-being, and this made the last two years extremely enjoyable and productive for me.

I am also greatly appreciative of the knowledge and support lent to me by Anna Robertson, Vickram Lakhian and Sean Cianflone. Their expertise with laboratory materials and methods was invaluable to my research. Further, their wealth of knowledge helped to spark experimental ideas, solve technical issues and generally guide my research direction. They all proved to be great sources of information and also great friends.

Additionally, I would like to thank the Civil Engineering administrative staff, namely Carol Robinson, for their tireless work and constant willingness to lend a helping hand. Her earnest kindness towards students made all office interactions a pleasure.

I would like to acknowledge my Masters committee, Dr. Yiping Guo and Dr. Younngy Kim, for their work reviewing and revising this thesis. Their time and expertise is appreciated.

Importantly, I would also like to acknowledge my friends and family for their immense support. Their love and friendship was always felt. My parents, especially, were key supporters of my academic ambitions. They supported me in countless ways, and I will forever be grateful. I only hope that I can exemplify their caring, patient, loving personalities in my own life.

Finally, I would like to thank Jess Doy, from who I drew not only motivation but also inspiration. She has supported me through two plus years of late night lab work, presentation induced stress and thesis writing blocks, all the while succeeding at pursuing her own dreams. Always quick to lend positive words of support, she knew how to calm my thoughts. In return, I can only humbly present her a fractured rock sample named in her honour…and my love.

Contents

List of Figures

List of Tables

List of Abbreviations

Below is a list of common acronyms.

ADE – Advection Dispersion Equation

APV – Average number of Pore Volumes required for particle elution

CFT – Colloid Filtration Theory

CM – Carboxylated Microsphere

CSTR – Continuously Stirred Tank Reactor

DLVO - Derjaguin-Landau-Verwey-Overbeek

ES – Electrostatic

HPLC – High Performance Liquid Chromatography

LB – Luria-Bertani

LCL – Local Cubic Law

PBS – Phosphate Buffer Solution

SCCE – Single Collector Contact Efficiency

VDW – VanDerWaals

List of Symbols

ρ – Fluid density

L – Fracture length

Pe – Peclet number

v – Fluid velocity

b – Fracture aperture

Q – Volumetric flow rate

g – Acceleration due to gravity

W – Fracture width

C – Concentration

μ - Dynamic viscosity

H – Hydraulic head

P – Pressure gradient

D_i – Dispersion coefficient

Re – Reynolds number

α_i – Dispersivity

D^* - Diffusion coefficient

a – Particle radius

d_p – Particle diameter

A – Hamaker Constant

K^{-1} – Debye length

ζ – Zeta potential

φ_i – Interaction energy

k – Boltzmann's constant

γ – Surface tension

T – Temperature (or Transmissivity)

τ – Mean residence time

V – Volume

N_D – Dispersion number

h_o – Minimum separation distance

ΔG – Interaction energy per unit area

ε – Permittivity of fluid transport media

d – Distance between particle/collector surface

Declaration of Academic Achievement

This thesis contains sections that have been prepared for submission to a peer-reviewed journal. These sections have been formatted according to McMaster School of Graduate Studies' guidelines for thesis containing such works. Chapter 3 has been written for journal submission. It was authored by J.G.L. Seggewiss and co-authored by S.E. Dickson. Rationale for its inclusion is as follows:

Ideas for experiments carried out in Chapter 3 were jointly developed by J.G.L. Seggewiss and S.E. Dickson. Experiments were carried out by J.G.L. Seggewiss. Data analysis was completed by J.G.L. Seggewiss, under supervision of S.E. Dickson. The journal manuscript was prepared by J.G.L. Seggewiss, while S.E. Dickson was responsible for editing. Work completed as explained in Chapter 3 allowed for significant conclusions to be drawn regarding the factors that affect particulate transport in single saturated fractures.

1.0 Introduction

1.1 Background

Bedrock aquifers are an important source of water for residential, agricultural and industrial use. Millions of people in Southwestern Ontario rely on bedrock aquifers for their potable water supply. The large majority of water from these aquifers is pumped from transmissive fractures within the bedrock, which can also function as pathways for biological and chemical contamination. Further, wells are often screened over large depths to ensure sufficient quantity of water is retrieved. This creates hydrological connections between geologic layers which can introduce contamination into previously pristine areas. Our increasing dependence on bedrock aquifers as potable water sources has amplified the urgency to understand, evaluate and quantify the impact of land use practices on these aquifers to try and understand the risks associated with contaminant transport through these aquifers. Several recent outbreaks of waterborne disease in North America have highlighted a lack of understanding about contaminant transport in the subsurface, particularly in fractured environments (e.g. Walkerton, ON, Penticton BC, Gideon MO, etc.) (Hrudey et al. 2003). The above-mentioned outbreaks all stemmed from groundwater sources; however, the pathogenic contaminants at the root of these outbreaks were different (e.g., rotavirus, *E. coli* and Norwalk-like virus). While Hrudey et al., (2003) recognized that disease outbreaks from groundwater sources are often due to extenuating circumstances (e.g., open, abandoned wells nearby, sewage backup near the wellhead, improperly identified GUDI wells), they suggested that these outbreaks were a potential catalyst to understanding contaminant transport in the subsurface.

Some early research into subsurface solute and colloid transport in fractured environments focused on characterizing the aperture size and colloid transport times (Mckay et al., 1993a; Mckay et al., 1993b). These studies helped to document the hydraulic transmissivity within fractured clay till using the local cubic law. Importantly, Mckay et al., (1993a) demonstrated that small, highly transmissive fractures can have a large effect on transport by drastically increasing the average groundwater velocity. Additionally, they hypothesized that smaller particles are subjected to diffusion into low flow zones and into the matrix, resulting in significantly decreased particle velocities, and were able to demonstrate this phenomenon

through quantifying the effect of colloid size on transmission speed. Collectively, these observations highlight the fact that geologic formations previously considered to be impermeable, such as clay and bedrock, can play an important role in contaminant transport. Further, this work demonstrates the dependence of particle transport on the size of both the particle and the aperture through which it is flowing.

Research into this area has expanded since this early work. Laboratory data sets, using real and synthetic rock fractures to examine the transport of inert tracers (bromide), biological contaminants (such as *E. coli*, MS2, PR772 and PRD1), and microspheres (both plain and carboxylated) of several sizes, have grown (Mondal & Sleep, 2013; Rodrigues et al., 2013; Schutten, 2012). This is in addition to field studies conducted analyzing contaminant transport through fractures, with a focus on the effect of networks (Becker et al., 2003; Munn, 2012; Novakowski et al., 2006). Together, these studies have identified several important characteristics influencing colloid transport in fractures, including the ionic strength and volumetric flow rate of the carrying solution, the fracture aperture and matrix porosity, and the size and surface properties of the particulate in the flow stream. All data are highly specific to the fracture formation, and therefore the resulting data are difficult to compare directly between experiments. Further, a complete data set analyzing the transport of bacteria, bacteriophage and microspheres has yet to be produced in order to further examine the effects of surface properties and particle size on transport.

1.2 Research Objectives

The goal of this work is to investigate the effects of particle surface properties, particle size, transport fluid ionic strength and aperture field characteristics on particulate transport through single saturated limestone fractures. Specifically, the effects of these properties on distinct transport and retention mechanisms will be considered. This will be achieved by generating effluent concentration profiles in a highly controlled laboratory setting, employing both biological and synthetic particles of several different sizes and surface properties (i.e. bacteria, bacteriophage and microspheres). This work will be conducted in two distinct limestone fractures with different aperture field characteristics. In addition to transport and retention mechanisms, the data collected through these experiments will enable a commentary on the appropriateness of microspheres as surrogates for microorganisms for particulate

transport in fractured rock environments. As more attention is paid to the risks posed by biological contaminants, information gleaned from research such as this will inform source water protection strategies and risk assessments.

1.3 Scope

This thesis contains three chapters in addition to this introduction (Chapter 1). Chapter 2 contains a thorough literature review of fluid and particulate transport in fractured media focusing on the physico-chemical mechanisms responsible for particle attachment, retardation, and channelling. Further, this chapter explores all current research avenues, analyzing efforts in the field, in the laboratory and from computer modelling work to understand the contributions of each. Chapter 3 contains a paper prepared for publication describing this work, including the motivation, objectives, methodology, observations, discussion and conclusions. Chapter 4 expands on these conclusions, with particular attention paid to recommendations for future work. Details regarding the experimental set up and methods are included in the appendices.

2 Literature Review

2.1Fluid Flow Through Fractures

The Navier-Stokes equations, based on the conservation of mass and momentum, provide the most rigorous and mechanistic description of fluid flow through fractures. In three dimensions, the Navier-Stokes equations are summarized as follows (Bird et al., 2002):

$$\rho(v \cdot \nabla)v = -\nabla P + \mu\nabla^2 v + \rho g \quad (1)$$

where ρ represents fluid density (kg/m^3), v is the fluid velocity in a given direction (m/s), P is the pressure gradient acting on the system in a given direction (Pa/m), g is the acceleration due to gravity (m/s^2) and μ is the dynamic viscosity of the fluid $(\mathrm{Pa{\cdot}s})$ (Bird et al., 2002). Equation (1) recognizes the impacts of inertial, pressure, viscous and gravitational forces on fluid movement. The left hand side of (1) represents inertial forces, and describes how the mass of fluid in a given volume is changing over time (Bird et al., 2002). The first, second and third terms on the right hand side of (1) represent fluid movement due to pressure gradients, shear forces and gravitational forces respectively (Bird et al., 2002). The derivation of (1) assumes Newtonian fluid, isothermal conditions, and an incompressible fluid. A complete derivation of (1) is provided by Bird et al. (2002).

Historically, computation of a three-dimensional flow field in a variable aperture fracture using Navier-Stokes has been too computationally intensive to solve at significant scales. This led to numerous simplifying assumptions resulting in several more simplistic models describing fluid flow through a fracture. The following paragraphs present each assumption and its implications on the flow equation. For reference purposes, Figure 1 shows the expected parabolic flow field development together with the coordinate system.

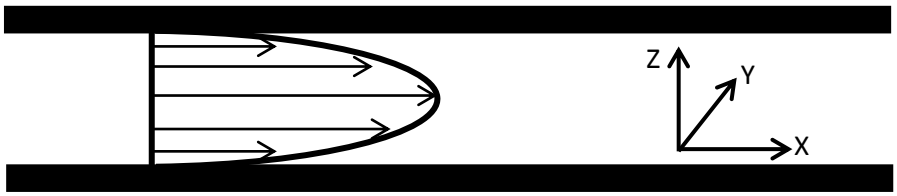

Figure 1 – Schematic diagram of a parallel plate fracture and the parabolic velocity profile together with the coordinate system.

If steady state conditions are assumed, the Navier-Stokes equations reduce to the following, known as the Stokes equation (Bird et al., 2002):

$$0 = -\nabla P + \mu \nabla^2 v + \rho g \quad (2)$$

In (2), the inertial forces describing fluid mass and velocity changes over time are considered negligible. The validity of this assumption is typically evaluated considering the Reynolds number to determine the flow regime as follows (Fox et al., 2009):

$$Re = \frac{\rho v L}{\mu} \quad (3)$$

where, ρ is fluid density (kg/m^3), μ is fluid dynamic viscosity (Pa·s), v is the characteristic fluid velocity (m/s) and L is the average aperture (m). While groundwater flow in fractures is commonly considered to be laminar, which makes steady state conditions a valid assumption, it should be noted that aperture fields are often highly variable and thus local regions of turbulence can develop (Brush & Thomson, 2003; Cardenas et al., 2007). Therefore, it is possible that the Stokes equation will not be valid in all aperture regions.

To simplify further, the assumption that the fracture walls slope gradually is invoked. As a result, fluid movement normal to the fracture surface is negligible. Viscous forces will occur only in the direction normal to fluid flow (the *z*-direction in Figure 1). Therefore, (2) can be simplified to the Reynolds equation as follows (Brush & Thomson, 2003):

$$0 = \mu \frac{\delta^2 v}{\delta z^2} - \nabla P \quad (4)$$

It is noteworthy that the fluid velocity still has *x* and *y* components in (4). Integrating across the aperture, perpendicular to the direction of flow, gives (Zimmerman & Bodvarsson, 1996):

$$\nabla \left(\frac{b^3 \rho g}{12\mu} \nabla H \right) = 0 \quad (5)$$

where b is the fracture aperture (m) and H represents the hydraulic head differential across the fracture length. This is the common form of the local cubic law (LCL) and still considers a pressure differential in two dimensions. If the fracture is likened to a set of parallel plates, the expected flow field is reduced to one-dimension, and the result describes the fluid velocity in the direction of flow as follows:

$$v = -\frac{b^2 \gamma}{12\mu} \frac{H_o - H_i}{L} \quad (6)$$

Equation (6) assumes that the fracture mid-surface is planar and that any variations in aperture are negligible relative to the aperture itself (Brush & Thomson, 2003). Finally, if the fracture

width is finite, the fluid velocity can be integrated across the aperture, perpendicular to the direction of flow, to the cubic law, which determines the volumetric flow rate as follows (Snow, 1965):

$$Q = \frac{-Wb^3 \rho g}{12\mu} \frac{\Delta h}{\Delta L} \tag{7}$$

where *Q* is the volumetric flow rate, *w* is the width of the fracture perpendicular to the direction of flow, *h* is the hydraulic head differential in the *x*-direction and *L* is the length of the fracture along the direction of flow.

Experimentally, the cubic law has proven to be very useful because it allows for an estimation of groundwater velocity through a variety of fractured media in a field setting (Cherry et al., 2006; Quinn, et al., 2011a; Quinn et al., 2011c). Due to its similarities with fractured rock, several studies have utilized the cubic law in a fractured clay setting (Cherry et al., 2006; Mckay et al., 1993a); however, these authors did acknowledge the limitations of the cubic law in their field applications. The largest limitation is that the parallel plate assumption is unlikely to occur in natural environments, and an appropriate 'representative' aperture is still under debate in the literature. Practically, the cubic law has also been used in a variety of packer tests to estimate fracture transmissivity and groundwater velocity (Quinn et al., 2011a; Quinn et al., 2011b; Quinn et al., 2011c).

Several recent studies have been able to use computer models to simulate three-dimensional fluid flow in variable aperture fractures using the Navier-Stokes equations. Notably, Brush & Thomson (2003) used simulated fractures to compare flow fields calculated by (1), (2) and (7), and suggested that inertial forces, typically assumed to be negligible, can have considerable influence on velocity profiles causing them to deviate significantly from the expected parabolic profile. They overlaid velocity profiles calculated using the Navier-Stokes, Stokes and Local Cubic Law equations, clearly demonstrating deviations from the local cubic law due to inertial forces and surface roughness. They found that deviations became larger with increasing fracture roughness, quantified using the coefficient of variation (COV) as:

$$COV = \frac{\sigma_m}{b_m} \tag{8}$$

where σ_m is the standard deviation of the aperture and b_m is the arithmetic mean aperture. Here, a COV of 0 represents parallel plates. Increased variance in the fracture field will increase the COV measure. Further, Brush & Thomson (2003) found the Reynolds number to be a useful measure of the validity of the local cubic law. Importantly, they noted that the volumetric flow rate across the entire fracture was not significantly different between the Navier-Stokes and local cubic law simulations under laminar flow conditions in fractures with small COV values. Therefore, while aperture-field variations may influence the velocity profile in localized regions, the volumetric flow through the fracture will not be significantly affected under these conditions.

Koyama et al. (2008) completed a simulation similar to that of Brush and Thomson (2003) to compare Navier-Stokes simulations directly with the local cubic law and Reynolds equation at different hydraulic gradients across the fracture. While this was a simplified two dimensional study, it also considered the effect of different flow fields on the transport of particles within the fracture. They demonstrated for Reynolds numbers ranging from 0.2 to 200, flow fields can be greatly influenced by the inclusion of inertial forces, particularly by considering vertical velocity components which are negated in the cubic law simplification. Additionally, they demonstrated that in areas of large vertical aperture change, the Navier-Stokes equations predicted some areas of negative velocity, indicating backwards flow. As a result of the flow field simplification carried out by the Reynolds equation, total flow rate was overestimated by 5-10%. Error was directly proportional to the Reynolds number. Importantly, they also studied the effects of flow fields on particle transport and found that under identical flow conditions (i.e. hydraulic gradient across the fracture); particle transport predicted by the Navier-Stokes equations was significantly slower (10-20%) than that predicted by the Reynolds equation, with increased variability. Therefore, they were able to quantify the importance of shear and inertial forces on particulate transport, again suggesting that the simplifications from the Navier-Stokes equations should be used with extreme caution.

2.2 Factors Affecting Particulate Transport

Water flowing through fractures may contain biological contaminants such as bacteria or viruses. These contaminants are represented as particulate material; their transport is dominated by the same mechanisms that would affect particles. Therefore, the understanding of

particulate transport is crucial to the understanding of the fate of biological contaminants within a fracture.

2.2.1 Advection Dispersion Equation

The main forces that govern particulate transport through a fracture are advection, mechanical dispersion, diffusion, adsorption, size exclusion, filtration, and other size-related effects. It is well documented that the mathematical terms describing these mechanisms can be combined into the Advection-Dispersion Equation (ADE) (Berkowitz, 2002; Ryan & Elimelech, 1996; Singhal & Gupta, 2010). The most dominant mechanisms affecting particulate transport are advection, mechanical dispersion and diffusion. Advection refers simply to the transport of a particle with the average fluid velocity in the primary direction of travel. The advective term in the ADE therefore relies only on the average fluid velocity in a given direction and the contaminant concentration. In three dimensions, the advective term is represented as follows (Fetter, 1999):

$$v \cdot \nabla \mathrm{C} = \frac{\partial C}{\partial t} \tag{9}$$

Diffusion is the motion of particles caused by concentration gradients between the immediate and surrounding fluid, and occurs in all directions regardless of the direction of flow. Mechanical dispersion refers to the spreading of particles due to the velocity gradient and different pathway lengths within the fracture, which are caused by the variability of the aperture field as well as the no-slip condition at the fracture walls. Aperture field variability can also lead to difference in the lengths of flow pathways. Together, advection, diffusion and dispersion affect the residence time of a contaminant in the fracture, and lead to both longitudinal and transverse dispersion. Both diffusion and mechanical dispersion cause particle transport distinctly different from that of advection. However, it is difficult to discern between these mechanisms and therefore they are often lumped together into one term, called hydrodynamic dispersion (Fetter, 1999). In porous media, transverse and longitudinal dispersion are typically represented respectively as (10) and (11). It is postulated that the same relationships exist in fractured media (Bauget & Fourar, 2008; Bear et al., 1993; Fetter, 1999).

$$D_L = \alpha_L v_i + D^* \tag{10}$$

$$D_T = \alpha_T v_i + D^* \tag{11}$$

where D^* is the diffusion coefficient (m^2/s), v is the velocity in the i^{th} direction (m/s), α is the longitudinal or transverse dynamic dispersivity (m), and D is the longitudinal or transverse dispersion coefficient (m^2/s). These equations assume that transverse particulate transport will occur equally in all directions, which is likely a safe assumption in fractured rock settings where the anisotropy common in porous media does not exist. The dispersivity term, α, is a constant dependent upon the media, and therefore can be difficult to determine.

The Taylor-Aris dispersion coefficient, initially developed for smooth-walled pipe flow, has been proposed as an alternative method of describing dispersion in variable aperture fractures (Bodin, et al., 2003). The Taylor-Aris dispersion coefficient is given as follows (Bauget & Fourar, 2008; Zheng, 2008):

$$D_h = D^* + \frac{v^2 b^2}{210 D^*} \tag{12}$$

where D_h is the hydrodynamic dispersion coefficient, v is the average fluid velocity and b is the fracture aperture. However, to properly use this equation, one-dimensional flow between parallel plates must be assumed. This is a similar assumption to the cubic law, and its validity may not always be assured.

A three dimensional ADE equation considering the major forces impacting particulate transport is given as follows (Ryan & Elimelech, 1996):

$$\frac{\partial C}{\partial t} = \nabla \cdot (D_h \cdot \nabla C) - \nabla \cdot (vC) \tag{13}$$

Here, the hydraulic dispersion is represented by D_h and can be directional. Further, V is the fluid velocity, and C is the contaminant concentration. Solving the full ADE analytically is a very difficult task, and leading research works to reduce the error of numerical solutions (Dehghan, 2004). Full numerical solutions of the ADE in three dimensions are possible, although difficult to compute in fractured environments. The ADE can be further reduced to a single dimension by assuming velocity and dispersion acting in one dimension only, as shown below.

$$\frac{\partial C}{\partial t} = \left(D_h \frac{\partial^2 C}{\partial x^2} \right) - \left(V \frac{\partial C}{\partial x} \right) \tag{14}$$

It is this form that several researchers have used to analyze the behaviour of specific particulates in both experimental and simulated environments (Bauget & Fourar, 2008; Mondal & Sleep, 2013; Odén et al., 2008).

The Peclet number is dimensionless and measures the ratio of advective to diffusive forces. The equation for the Peclet number is shown as (15), and can help to determine the relative importance of each term in the ADE (Bauget & Fourar, 2008; Ohman et al., 2004).

$$Pe = \frac{vL}{D_h} \tag{15}$$

While advective and dispersive forces adequately describe the most influential mechanisms of transport within a rock fracture, several other factors do exist and must be considered in the transport of particulates. Most importantly, this includes: adsorption, size/charge exclusion, retardation, filtration and decay.

2.2.2 Particulate Adsorption

The attractive and repulsive forces acting between the particle and the fracture wall often predict attachment of the particulate material. Comprehensively known as the Derjaguin-Landau-Verwey-Overbeek (DLVO) theory, attractive VanDerWaals forces are opposed by electric double layer (EDL) repulsion (Tufenkji & Elimelech, 2004). In this particular case, if the fracture is considered to be a flat plate and the particle is assumed to be spherical, the attractive and repulsive forces can be approximated respectively as (Bos et al., 1999):

$$\varphi_a = -\frac{A}{6}\left(\frac{a}{d} + \frac{a}{d+2a} + \ln\left(\frac{d}{d+2a}\right)\right) \tag{16}$$

$$\varphi_r = \pi\varepsilon a(\zeta_1^2 + \zeta_2^2)\left(\frac{2\zeta_1\zeta_2}{\zeta_1^2+\zeta_2^2}\ln\left(\frac{1+\exp(-\kappa d)}{1-\exp(-\kappa d)}\right) + \ln(1-\exp(2-\kappa d))\right) \tag{17}$$

where, ζ is the zeta potential of a given surface or sphere (V), κ^{-1} is the Debye length (m), a is the particle radius (m), A is the Hamaker constant (J), d is the distance between the particle and fracture surface (m), ε is the permittivity of fluid transport media (F/m), φ_a is the predicted attractive energy due to the VanDerWaals forces (J), and φ_r is the repulsive force as predicted by the EDL (J).

The DLVO theory can be used to predict several complex mechanisms within rock fractures, including the development of secondary energy minimum, which is a distance between the particle and fracture wall at which the particles will attach to the fracture wall in a lower energy state. Literature has shown attachment in the secondary minimum to be reversible (Mondal & Sleep, 2012; Redman et al., 2004; Tufenkji & Elimelech, 2004). While (16) and (17)

provide the best approximation available, they do not consider the effect of high salt concentrations on the system, especially in the presence of an air phase. As detailed by Boström et al. (2001), the DLVO theory may become ineffective for predicting interaction energies when salt concentrations become high in the presence of an air phase. However, under saturation conditions the DLVO theory is a useful tool for approximating and understanding the adhesion between particles under non-favourable (like charged) conditions.

It is widely accepted that adhesion between like charged particles can occur at relatively low interaction energies due to the secondary energy minimum (Boström et al., 2001; Tufenkji & Elimelech, 2004). DLVO theory is expected to be especially useful when considering bacteriophage and microsphere transport, as these materials are considered more likely to conform to the spherical shape assumption. Some literature suggests that the DLVO theory underestimates the actual adhesion of particles to fracture media under unfavourable conditions because it does not accurately describe all forces (Ryan & Elimelech, 1996). Deviation of experimental results from predicted DLVO behaviour has induced several attempts to explain this behaviour. Some suggest this could be due to surface charge heterogeneity, particle surface roughness or fracture surface roughness, which might all act to increase particulate adsorption (Lakkapragada & Walz, 1996; Ryan & Elimelech, 1996). Shen et al., (2012) were able to show definitively in their simulations that increased wall surface roughness promoted spherical particle adhesion to that wall. Further, they found that under unfavourable adhesion conditions, retention within the secondary energy minimum was more likely than in the primary minimum, potentially making it reversible.

Contrary to this, others contend that the DLVO theory as proposed is not complete, and can be modified to include additional attractive and repulsive forces (Grasso et al., 2002; Redman et al., 2004; Syngouna & Chrysikopoulos, 2013; Tufenkji, 2007). Often, extended DLVO forces are attributed to colloid hydrophobicity (Grasso et al., 2002). Grasso et al. also suggest that hydrophobic forces are related to hydrogen bonding within the fluid and therefore can be quantified through Lewis acid/base interactions.

2.2.3 Size/Charge Exclusion and Filtration Mechanisms

Size exclusion and particle straining will also affect particle transport and retention. They are both dependent on the size of the particle, and therefore have been grouped in this section.

In a parallel plate fracture, a velocity profile will develop across the fracture, as depicted in Figure 1. However, large sized particles will be restricted from moving towards the extreme low flow areas near the fracture wall by virtue of their size (Zheng, 2008). As a result, particles are expected to have a larger average velocity when traveling through a saturated fracture relative to solute flow (Abdel-Salam & Chrysikopoulos, 1995). Similarly, particles may be restricted from entering low flow areas of the fracture due to their physical size if the fracture aperture reduces significantly in size at the entrance to the low flow area. This would cause particles to remain in regions with larger, preferential pathways, again increasing the expected average linear velocity (Burke, 2012; Mondal & Sleep, 2012). The particle may also be mechanically removed from the stream through a straining process, which would occur if the particle is larger than the aperture region through which it is being transported (Redman et al., 2004; Tufenkji, 2007).

Charge exclusion refers specifically to repulsive forces that work to keep particles in high velocity regions of the flow stream, and away from the low velocity regions near the fracture wall (Burke, 2012). This could be due to interactions with the fracture wall itself, or interactions with a previously deposited particle (Bos et al., 1999). A simplistic example of a particle in the stream interacting with a previously deposited particle is shown in Figure 2. Here, the charge interaction between the two particles causes the non-deposited particle to be pushed away from the fracture wall where the average velocity is higher.

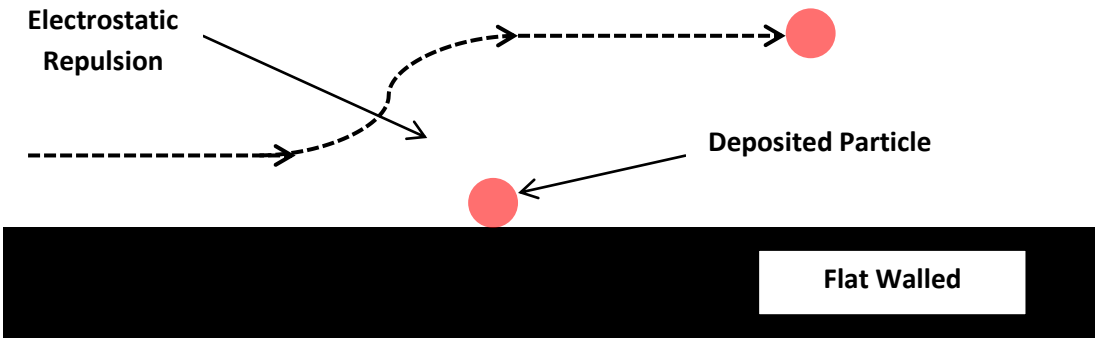

Figure 2 - Schematic representation of charge exclusion causing increased average velocity of a particle

Straining, size and charge exclusion can also restrict the particle from diffusing into the rock matrix (Zvikelsky & Weisbrod, 2006). The transmissivity of the rock matrix is typically orders of magnitude lower than that of the fracture. Solutes that are able to diffuse into the rock matrix have been shown to have long release times as they diffuse back into the main stream when the concentration gradient reverses (Freeze & Cherry, 1979; Mckay et al., 1993b).

Within the fracture, there are four mechanisms that may result in the adsorption of particles onto the fracture surface. Similar to porous media, straining, sedimentation, interception and diffusion may all cause the particle to contact the fracture surface (Zvikelsky & Weisbrod, 2006). Further, it has been predicted in porous media theory (Crittenden, et al., 2005) and shown in rock fracture literature (Zvikelsky & Weisbrod, 2006) that the contact mechanism and efficiency may directly depend on the particle size. The extension of this theory with respect to biological colloids has yet to be made.

Sedimentation may result from the settling of particles out of the flow stream should their density be larger than that of the fluid in which they're flowing (Zvikelsky & Weisbrod, 2006). However, some biological content, like viruses and bacteria, have very similar densities to that of water (Zheng, 2008). Therefore, sedimentation by gravity is often not considered. Should it be applicable, gravitational sedimentation is frequently modelled using Stokes settling velocity, which assumes laminar flow. The equation is as shown below:

$$v_s = \left(\frac{1}{18\mu}\right)(\rho_p - \rho_f)(g d_p^2) \qquad (18)$$

where ρ is the density of the particles or fluid (kg/m^3), g is the gravitational constant (m/s^2), d_p is the particle diameter (m) and μ is the fluid dynamic viscosity (Pa·s).

2.2.4 Retardation Eddies and Decay

The existence of fluid eddies and biological decay are two additional mechanisms that do not cause the adsorption of particulate material, but may be interpreted as such. Local eddies may form due to the complex nature of fracture apertures. Particles can become trapped in these eddies resulting in delayed transport. This mechanism may result in large tailing portions of effluent concentration profiles (Cardenas et al., 2007; Singhal & Gupta, 2010). Importantly, due to the heterogeneous nature of fracture apertures, areas of turbulence and eddying can occur even under relatively laminar flow conditions. Current research is addressing this topic and attempting to quantify the significance of this effect on particulate transport through the use of computer simulations. Moreover, radioactive or biological contaminants may decay during transport through the fracture and therefore not be quantified in the effluent stream. It becomes very difficult to discern between mechanisms (i.e. adsorption vs. survival or decay) when considering simple effluent concentration curves. Steps should be taken to mitigate the

misinterpretation of biological decay through the use of inactivation experiments, which quantify the viability of biological material over time.

2.3 Modelling Retention

Often, all of the above factors are lumped together into a modified ADE equation (Ryan & Elimelech, 1996):

$$\frac{\partial C}{\partial t} = \nabla \cdot (D \cdot \nabla C) - \nabla \cdot (VC) - \frac{D \cdot F}{kT} C \tag{19}$$

where F is the sum of DLVO and gravitational forces acting on the particle, D is the diffusion coefficient (m^2/s), k is Boltzmann's constant ($m^2 \cdot kg/s^2 \cdot K$) and T is the temperature (K). This last term makes (19) unique from other representations of the ADE by considering the adhesion of particles to the material. F is further described as follows:

$$F = F_G + F_{par} \tag{20}$$

$$F_{par} = -\nabla \varphi_{tot} = -\nabla(\varphi_a + \varphi_r) \tag{21}$$

where φ_a and φ_r are the attractive VanDerWaals and repulsive electrostatic forces (J) respectively, as described by (16) and (17). Alternatively, the last term in the ADE equation describing the attachment of particles in fractures may be modelled by a probability distribution as follows (James et al., 2005):

$$p_a = \exp\left(-\frac{\varphi_r}{kT}\right) \tag{22}$$

where p_a is the probability of particle attachment, φ_r is the energy of repulsion (J), k is Boltzmann's constant ($m^2 \cdot kg/s^2 \cdot K$) and T is the temperature (K). James et al. (2005) recognized that this probability term can be adjusted if more specific information is known about a given system as this retention term will be variable depending on both the particle and the media through which it is traveling. Several studies have recognized this as a shortcoming in current research concerning flow through fractures, noting this term could potentially be modified, but knowledge of the interaction between different contaminants and different rock materials is first required (Berkowitz, 2002; James et al., 2005).

Theoretically, the advection-dispersion equation can be solved to find a retention rate of particles in the fracture. However, (19) is often reduced to a one dimensional problem in order

to facilitate its solution (Bakker et al., 2002; Ryan & Elimelech, 1996). For example, the Von Smoluchowski-Levich approximation considers attractive VanDerWaals forces to be balanced by the hydrodynamic drag that acts on a stationary particle in a fluid (Bakker et al., 2002). It has been used previously to describe the adhesion of bacteria to a smooth surface. However, this approximation does neglect repulsive electrostatic forces, and therefore is often considered the maximum deposition rate possible (Bakker et al., 2002). Thus, the Von Smoluchowski-Levich approximation often over-estimates the particle attachment rate. The ratio between the actual deposition rate and the maximum deposition rate can be considered the efficiency of deposition (Zheng, 2008), where the actual deposition rate can be observed in a highly controlled experiment using parallel plates and image analysis (Zheng, 2008).

2.4 Aperture Characterization and Effects of Aperture Variability

As previously acknowledged, several particle transport mechanisms are affected by the aperture size and variability, including mechanical straining and particle interactions with the fracture wall. Therefore, it is very important to characterize both the average aperture and the aperture field variability across the field of study. There is also a distinct difference between fieldwork, laboratory studies and computer simulations with respect to the detail in which apertures are described.

2.4.1 Computer Simulated Rock Fractures

Some computer simulations use the previously described Navier-Stokes equations to evaluate two-dimensional fluid transport within a fracture. However, in order to carry out this simulation, fracture apertures at each calculation location (i.e. node) must be well defined. Therefore, synthetic fractures are often generated, through which fluid flow and particulate transport can be simulated. Alternatively, real fractures can be scanned and their data employed in simulations. Brush & Thomson, (2003) generated simplistic sinusoidal shaped fractures and rough-walled fractures to investigate flow. They were able to confirm the importance of Reynolds number on the laminar flow assumption made by the creeping flow and local cubic law equations.

Cardenas et al., (2007) imported an X-ray scanned fracture into COMSOL (a finite element analysis software package) to evaluate the existence of non-linear flow regions and the effect on particulate transport in fractures in two dimensions They used Navier-Stokes equations

to define the velocity profile within the fracture, then used this information as an input into the ADE to determine particulate transport. They found that the assumption of a uniform fracture (as per the local cubic law) significantly increased the modeled flux of contaminant concentration, perhaps due to the absence of recirculation zones caused by fracture roughness. Concentrations within these zones were shown to be relatively immobile, helping lead to exaggerated tailing on outlet concentration curves. Similar findings in two dimensions using Navier-Stokes equations to describe fluid flow are shown by Koyama et al., (2008).

Instead of using real fractures, several studies have generated log-normally distributed fractures to investigate transport (James et al., 2005; Zheng et al., 2009). These studies generated flow field from the Reynolds equation, and used random walk particle tracking to simulate particle transport. Using this approach to simulate both fractures and particulate transport, James et al., (2005) and James & Chrysikopoulos, (2000) explored the effects of attachment onto the matrix, diffusion into the matrix, and aperture variability on particle transport. Using generalized expressions for both diffusion and adsorption, these studies have demonstrated increasing retardation with increasing aperture variability and favourable attachment conditions. James et al., (2005) and James & Chrysikopoulos, (2000) acknowledge that their simulations are based entirely on manufactured systems, however they argue that the trends shown in their simulations would hold in real systems as well. Further, they suggest that more accurate representations of specific systems could be made with customized parameter estimation.

2.4.2 Field Methods of Aperture Calculation and Characterization

In a field setting, fractures are characterized in a much different manner than in a lab or model setting. It is impossible to fully characterize an in-situ fracture due to its complexity and a lack of non-destructive characterization techniques. Current techniques still rely on the construction of boreholes, which may inherently alter the properties of the part of the fracture abutting the drilling line. Data regarding fractures intersecting the borehole are collected through core logging and down-hole geophysics. Acoustic televiewers (ATV) estimate the frequency, size and pitch of fractures intersecting the borehole (Munn, 2012; Pehme et al., 1999). However, ATV logs can occasionally be misleading since they do not identify closed fractures (those with no hydraulic activity) and may not identify very small fractures. Therefore,

the ATV log is typically supplemented with hydraulic tests, such as step tests and slug tests, that can be used to calculate the transmissivity of an isolated fracture (or set of fractures) (Quinn et al., 2011a; Quinn et al., 2011c). Alternatively, fracture transmissivities can also be approximated through the installation of the FLUTe borehole liner. Transmissivities are then correlated to the local cubic law to approximate an equivalent aperture of the fracture or series of fractures as follows (Quinn et al., 2011c):

$$b = \left(\frac{12\mu T}{N\rho g}\right)^{\frac{1}{3}} \tag{23}$$

Where T represents the measured transmissivity (m^2/s), N is the number of fractures over the measured interval, g is the gravitational constant (m/s^2), ρ is the fluid density (kg/m^3) and b is the fracture aperture (m).

Consideration of scale is important at field sites, as fracture networks and hydraulic connections between fractures render the properties of an individual fracture less important. Further, for the purposes of contaminant tracking and transport, it is important to understand the hydraulic connections between fractures at different elevations. Boreholes can hydraulically connect fractures and provide conduits for contaminant transport.

2.4.3 Lab Setting Aperture Calculation and Characterization

Although not possible in a field setting, the nature of working with a fracture in the lab allows for a more thorough characterization of the fracture. In a review paper, Tsang (1992) consolidated the inconsistent terminology in the literature into three distinct equivalent apertures: the mass balance, frictional loss and cubic law apertures. These terms have subsequently been utilized in experimental work to characterize the variability of each fracture (Rodrigues et al., 2013; Zheng et al., 2008). This section defines the equivalent apertures classified by Tsang (1992).

Equation (7) can be rearranged to solve for the cubic law aperture, b_c, as follows:

$$b_c = \left(\frac{12\mu QL}{\rho g W \Delta h}\right)^{\frac{1}{3}} \tag{24}$$

As discussed in Section 2.1, (24) is developed directly from the cubic law assuming that the fracture behaves as a set of parallel plates. The cubic law aperture is the most widely used

because it only requires the head loss across the length of the fracture. Therefore, it is also referred to as the hydraulic aperture.

The remaining equivalent apertures are calculated using data derived from the effluent concentration profiles measured from solute tracer experiments. The mass balance and the frictional loss apertures are detailed as follows, respectively:

$$b_m = \frac{Q\tau}{LW} \tag{25}$$

$$b_f = L\left(\frac{12\mu}{\rho g(\Delta h)\tau}\right)^{\frac{1}{2}} \tag{26}$$

where Q is the volumetric flow rate (m^3/s), W is the fracture width (m), L represents the length of the fracture (m), μ is the dynamic viscosity of the liquid (Pa·s), τ is the average residence time (s), h is the head difference (m), ρ is fluid density (kg/m^3) and g is the gravitational constant (m/s^2). It is expected that these aperture calculations will not be equal, and therefore provide some insight into the variability of the aperture field. It is expected that the mass balance aperture (b_m) will be the largest of the three equivalent apertures, as it is based on the mean residence time of the mass, and larger aperture regions store more mass than smaller aperture regions. It has been argued (Tsang, 1992) and demonstrated (Zheng et al., 2008) that the mass balance aperture provides a good representation of the arithmetic mean aperture. b_f and b_c, however, are both influenced by the measured head loss across the fracture, assuming laminar flow, which is controlled by the smallest aperture regions. Between these estimations, the cubic law aperture (b_c), a representation of the geometric aperture average, is expected to be larger than the frictional loss aperture (b_f).

An additional aperture measurement technique, called direct aperture field measurement, was demonstrated by Zheng et al. (2008) when they measured the intensity of transmitted light at each point in a transparent fracture cast. Using the beer-lambert law, the measured intensity was correlated to an aperture size at each pixel.

2.5 *Escherichia coli* Characteristics

Escherichia coli (*E. coli*) is a rod shaped bacteria with a typical length of approximately 2.5 µm and diameter of 0.8 µm (Passmore et al., 2010). Generally, *E. coli* is a gram negative bacteria that is frequently used as an indicator of fecal contamination in a water source

(Tchobanoglous et al., 2003). Multiple references have shown the measured electrophoretic mobility of the *E. coli* to be negative, although the magnitude of this measurement is debated and shown to be dependent on the ionic strength of solution (Passmore et al., 2010; Soni et al., 2008; Walker et al., 2004). These references also show electrophoretic mobility measurements to be independent of growing conditions. While it has been suggested that the complex surface of biological material makes the zeta potential calculation inaccurate for this situation (Langletet al., 2008), other research shows that a relationship still exists between the ionic strength of solution and deposition of bacteria in a packed bed column (Walker et al., 2005). Therefore, while perhaps more complex, a relationship still likely exists between the ionic strength of solution and bacterial attachment. Some strains of *E. coli* are pathogenic, such as the O157:H7 strain that was found to be responsible for the water contamination tragedy in Walkerton, Ontario in 2000 (Hrudey et al., 2003).

In a fractured crystalline rock setting, Becker et al., (2003) achieved low recovery of a wide variety of bacteria, including those which were gram negative and rod shaped. They also found that motile bacteria had relatively lower recoveries than non-motile bacteria, suggesting that the added surface features on motile bacteria increase the probability of it being retained within a fracture.

In a laboratory setting, *E. coli* RS2G has been utilized to study the transport mechanisms of *E. coli* in both real dolostone fractures and synthetic replicate fractures. The nature of the bacteria has been used to run visualization experiments, in which the transport of bacteria is observed through the transparent replicates of laboratory-scale fractures (Burke, 2012; Rodrigues, 2012). These experiments also investigated the effect of different flow rates and different aperture fields on *E. coli* transport. It was determined that both the increased variability in the aperture field and an increased flow rate increased the retention within the fracture (Burke, 2012; Schutten, 2012). These experiments, however, were conducted under relatively favourable attachment conditions, using a transport solution with high ionic strength.

2.6 Bacteriophage MS2

MS2 is a coliphage, meaning it is a virus that will infect *E. coli* only. Specifically, MS2 is a single stranded RNA virus particle with an icosahedral shape (Grabow, 2001). Its equivalent diameter is approximately 24 nm (Guan et al., 2003). Further, literature suggests that

temperature will have an effect on virus viability, while other factors (such as water pH) are negligible (Yates et al., 1985). MS2 is expected to carry a slightly negative charge as measured by the electrophoretic potential; however, the applicability of this charge is debatable due to the nature of the complex surface of MS2.

MS2 has been used extensively in both field studies and laboratory experiments as a surrogate for pathogenic virus material of similar sizes. Although working in clay till, McKay et al. found that MS2 bacteriophage could be utilized to trace fractures within the soil (Mckay et al., 1993c). Importantly, they found that MS2 (and other bacteriophages) exhibit markedly different transport behaviour from conservative solute tracers, migrating through their experimental fractures significantly faster than solutes. Ojha et al., (2011) also commented on the ability of bacteriophage material to move quickly through rock fractures relative to porous media, where the average velocity of water is generally slower. Further to this, they demonstrated through simulations using the ADE that both matrix porosity and inactivation constants can affect the expected effluent concentration of bacteriophage in both fractured and porous media. Therefore, it is very important to consider these factors when analysing MS2 transport. Frazier et al. (2002) looked at the vertical transport of biological and solute constituents in weathered granite bedrock. They were able to confirm the rapid transport of bacteriophage through fractured material. They also showed the inability of MS2 to migrate into the rock matrix relative to a bromide tracer.

Mondal & Sleep, (2013) investigated the effect of solution conductivity and particle size on transport conditions using MS2 as a tracer material within dolomite rock fractures at the laboratory scale. They found that increasing ionic strength and ion valence promoted attachment to the fracture wall. Although the validity of zeta potential calculations has been questioned, these results suggest some DLVO type forces are influencing particle transport within the fracture. Additionally, this work suggests MS2 transport can be predicted using one-dimensional modelling software incorporating attachment, detachment and decay. Finally, they commented on the differences in transport between MS2 and similarly sized microspheres, suggesting that steric repulsion is responsible for observed differences in retention.

2.6 Microspheres

Several studies have utilized microspheres as a surrogate for bacterial transport in both laboratory and field settings. In a lab setting, Mondal & Sleep, (2013) compared the transport characteristics of microspheres to bacteriophage material and found that bacteriophage transport was best replicated by relatively larger microspheres. Similar work by the same authors was able to show the importance of ionic strength on the retention of microspheres within a dolomite fracture. Importantly, they were also able to elute microspheres from the fracture by simply altering the solution conductivity from 12 mM to 1 Mm (Mondal & Sleep, 2012). At high solution conductivities, they predicted the presence of a secondary energy minimum using the DLVO theory. By altering solution conductivity, they effectively changed the energy profile, eliminating the secondary energy minimum and theoretically promoting the elution of all particles previously adhered to the fracture within this minimum. Therefore, this work supports current electrostatic theories for adhesion within the fracture.

Cumbie & McKay, (1999) were able to show that within a shale saprolite environment, an ideal microsphere size exists that balances diffusion and settling characteristics to result in the highest percent recovery. The actual percent recoveries communicated from this work are very low relative to those observed in fractures, indicating that the filtering effect of the porous media is significant. The applicability of this idea to a purely fractured media environment has been suggested but not thoroughly tested (Mondal & Sleep, 2013).

The idea of an ideal particle size for transport was supported by the findings of Zvikelsky & Weisbrod, (2006), although the exact ideal particulate sizes were not exactly as predicted above. Work was completed in fractured chalk rock cores, and also confirmed previous observations correlating larger particulate sizes with quicker transport times.

Summary of Paper: *Mechanisms affecting the transport and retention of E. coli, MS2 and carboxylated microspheres in laboratory-scale saturated fractures.* (Prepared for submission to Environmental Science and Technology)

3.0 Mechanisms affecting the transport and retention of bacteria, bacteriophage and microspheres in laboratory-scale saturated fractures

Abstract

Particulate transport through saturated fractures is an emerging focus of research that can contribute to the determination of posed to groundwater. This research aimed to determine the importance of several retention and retardation mechanisms by examining the effect of ionic strength, particulate size and particulate surface properties on transport through single, saturated dolomite fractures. experiments were conducted using a conservative tracer (bromide), carboxylated microspheres (42.5 and 525 nm), and biological particulates (MS2 and *E. coli*). It was found that aperture size and variability had a large effect on particulate transport, with larger, more variable fractures leading to increased transport times over similar distances. However, increased variability was also associated with decreased retention within the fracture. Altering the ionic strength mid test resulted in minimal additional elution of particulate material, suggesting retention within the secondary energy minimum is negligible. Therefore, the large discrepancy observed between retention of biological particulates and carboxylated microspheres is likely due to distinct surface characteristics and biological surface heterogeneity. Overall, this work suggested that carboxylated microspheres are subjected to different retention mechanisms than biological particles, and are therefore poor surrogates for biological transport.

3.1 Introduction

Groundwater is an important resource for provision of drinking water, agricultural irrigation and industrial water needs. Tragedies related to contaminated drinking water sources (e.g. Walkerton, 2000, etc.) have poignantly demonstrated a lack of understanding of particulate transport through fractured media, and have provided motivation to study the transport of particulates in the subsurface (Hrudey et al., 2003). Research in this area has developed at

several scales, including: field, laboratory, and computer simulations using both real and simulated fractures.

Fluid transport through fractures is mathematically described by the Navier-Stokes equations. Simplifying assumptions are typically applied to these equations to make computation much easier. This results in several other equations describing fluid transport, such as the local cubic law. Brush & Thomson (2003) simulated three dimensional flow in computer-generated fractures using the Navier-Stokes equations and demonstrated, quantitatively, that the laminar flow and parallel plate assumptions commonly employed in the Stokes and local cubic law simplifications do not incorporate areas of local turbulence. These findings were supported by the work of Cardenas et al., (2007), who completed two dimensional simulations of real fractures and demonstrated that drastic changes in topography could lead to the formation of local eddies. Dispersion or diffusion into these zones could significantly affect particulate transport through increased retention or residence time.

Interest in the transport of particles in fractures heightened when Mckay, et al., (1993b) demonstrated that particles have significantly increased groundwater velocities relative to solutes. Since then, a body of research has developed with a focus on identifying potential mechanisms affecting the transport and retention of particles within fractured media. Laboratory work has isolated particular factors affecting transport, such as particle size, ionic strength and fracture roughness to try and quantify the effect of these variables on transport and retention of particles (Mondal & Sleep, 2013; Zheng et al., 2009; Zvikelsky & Weisbrod, 2006).

The Advection-Dispersion Equation (ADE) is commonly used to describe and model particulate transport within fractured media. The basic form of the ADE captures particulate transport due to fluid flow (advection), concentration gradients (diffusion) and velocity gradients across the flow field (dispersion). Modifications to the ADE have been made to capture retention of particulate material within a fracture. Several researchers have suggested these mechanisms could include adhesion, sedimentation, straining and decay (Mondal & Sleep, 2013; Rodrigues et al., 2013; Zheng, et al., 2009; Zvikelsky & Weisbrod, 2006). Previously, adhesion has been described using the Derjaguin-Landau-Verwey-Overbeek (DLVO) theory, which balances attractive VanDerWaals (VDW) forces with repulsive electrostatic (ES) forces to predict

particulate energy interactions at the collector surface. DLVO theory has been extensively examined in porous media situations, where the importance of the secondary energy minimum has been observed (Redman et al., 2004; Tufenkji & Elimelech, 2005). With respect to fractured media, Hoek & Agarwal (2006) investigated the effect of surface roughness on DLVO interactions. Using simulations, they suggest that rough surfaces may increase retention of particles within the fracture. This positive correlation between surface roughness and particle retention was confirmed by Darbha, et al. (2010), who examined the deposition of latex microspheres on a calcite surface. On a local scale, the energy profile is expected to be best described by the interaction between a spherical particle and a plate. Equations describing the VDW and ES forces in this scenario are given by Bos et al., (1999) and reproduced as follows.

$$\varphi_a = -\frac{A}{6}\left(\frac{a}{d} + \frac{a}{d+2a} + \ln\left(\frac{d}{d+2a}\right)\right) \tag{27}$$

$$\varphi_r = \pi\varepsilon a(\zeta_1^2 + \zeta_2^2)\left(\frac{2\zeta_1\zeta_2}{\zeta_1^2 + \zeta_2^2}\ln\left(\frac{1+\exp(-\kappa d)}{1-\exp(-\kappa d)}\right) + \ln(1-\exp(2-\kappa d))\right) \tag{28}$$

where ζ is the zeta potential (V), κ^{-1} is the debye length (m^{-1}), a is the radius of the spherical particle (m), d is the distance between the fracture surface and particle (m), ε is the permittivity of the transport media (F/m), φ_r and φ_a are the calculated attractive and repulsive energies, respectively (J). This is often standardized into a unitless number for easy comparison by dividing by kT, where k is boltzmann's constant (J/K) and T is the temperature (K).

The importance of ionic strength on particulate transport through fractures has been previously explored by Mondal & Sleep, (2012, 2013), Rodrigues & Dickson, (2013) and Rodrigues et al., (2013). Mondal & Sleep, (2012, 2013) conducted a series of laboratory-scale experiments, passing several different sized carboxylated microspheres and MS2 through a single saturated fracture. They found that altering carrying solution conductivity affected the ultimate recovery of particulates they observed. Generally, increasing ionic strength decreased the particle recovery. Further, they demonstrated that elution of adsorbed microspheres was possible by drastically reducing the ionic strength of the carrying solution. This was due to the effect of ionic strength on the interaction between particle and fracture, as described by the DLVO theory. However, these studies did not attempt to elute MS2 adhered to the fracture. Rodrigues & Dickson (2013) detailed the transport of particulate material through fractures and

drew general conclusions regarding retention based on: matrix charge, particle zeta potential, particle surface area, ionic strength of carrying solution, specific discharge and diffusion coefficient. It was found that the most significant characteristics for retention depended on the ionic strength of carrying solution, surface potentials of the particulate and fracture, and the Peclet number (which describes the ratio between advective and diffusive transport). This work considered the results of numerous experiments passing particulate material through single, saturated fractures. Specific mechanisms of particle retention were not explored in this work.

Other important factors affecting particle transport through fractured media are the particle size and particle type. Mondal & Sleep (2012, 2013) speculated that retention differences between particle types could be caused by either size discrepancies or different surface properties, the latter being the most likely given that MS2 and microspheres reacted differently to changing ionic strength conditions. Overall, microspheres were found to be poor surrogates of viral travel. Comparison to other types and sizes of biological particles, such as *E. coli*, was not considered in their work. Qu (2010) and Schutten (2012) both completed detailed work examining the effect of particulate size and specific discharge on particulate retention within single fractured rocks. Generally, increased residence time for smaller particles was observed, and increased retention occurred in experiments conducted at higher specific discharges. It was also found that biological particles resulted in much greater variability between experiments under identical experimental conditions, relative to microspheres, alluding to the sometimes erratic behaviour of biological particulate material.

Mondal & Sleep (2012, 2013) also give some attention to the comparison of fractured media to porous media, and the use of filtration theory to explain observable differences in particulate retention. The one dimensional ADE equation was fit to breakthrough curve data gathered in fractured media. It was found that the data were well represented. It was commented that attachment and detachment rates used for fitting were similar to those found considering the transport of MS2 through porous media using a two-site kinetic model, like that employed by Schijven et al. (2002). Mondal & Sleep (2012, 2013), further postulated that differences in retention observed between microspheres and MS2 could be explained using colloid filtration theory (CFT). Foppen & Schijven, (2006) describe the single collector contact efficiency (SCCE) as a measure of particulate collision and retention within a porous media

setting. Tufenkji & Elimelech, (2004) develop an equation to calculate the SCCE based on the main transport mechanisms of diffusion, sedimentation and interception, while also considering Van der Waals and hydrodynamic forces. Mondal & Sleep (2013) used the SCCE equations as proposed by Tufenkji & Elimelech (2005) to calculate a much greater SCCE for the small microspheres relative to the large ones, therefore resulting in increased retention. The increased SCCE was largely attributed to the increased diffusion associated with smaller particles, as predicted by the Stokes-Einstein equation. However, the differences in surface properties and their effect on particle retention and applicability to filtration theory were not explicitly explored.

Previous studies have identified important particle characteristics that affect transport and retention mechanisms in fractured media. However, a complete data set considering the transport of microspheres, MS2, and *E. coli* through the same single saturated fracture, enabling the isolation of independent retention mechanisms, does not exist. The goal of this work is to elucidate the effect of particulate surface properties, particle size, transport fluid ionic strength and aperture field characteristics on particulate transport within single, saturated rock fractures. This will be accomplished using two different sizes of microspheres (diameters of 0.0425 µm and 0.525 µm) and two different types of biological particulates (MS2 and *E. coli* RS2GFP). Within a highly controlled laboratory setting, these materials will be passed through two sample rock fractures with different aperture characteristics and the effluent concentration curves, from which percent recovery and average residence times can be calculated, will be measured. Data garnered from these experiments will provide insight into the relative importance of different retention mechanisms within fractured media under different experimental conditions. Further, it will enable comment on the validity of using microspheres as a surrogate to biological particulate transport.

3.2 Materials and Methods

3.2.1 Rock Fractures and Experimental Set Up

Two dolomite rock samples were collected from the Dolime quarry in Guelph, Ontario; one from the Guelph Formation and the other from the Eramosa Formation. These samples were cut into rectangular prisms and single fractures were induced in these samples by applying a uniaxial load. The two long edges of the fracture were then sealed, effectively creating no flow

boundaries. Over the time period considered, diffusion into the rock matrix is not a significant transport mechanism (Rodrigues et al., (2013)). Therefore, particulate transport is only considered within the fracture itself for this work. Figure 3 shows a schematic diagram of the experimental set up. Upstream and downstream flow cells were constructed, attached to the shorter edges, and sealed. These flow cells included a recirculation system run by a peristaltic pump. This allowed each flow cell to be modelled as a continuously stirred tank reactor (CSTR), from which exact influent and effluent concentrations could be calculated. Each recirculation system also included a sampling vial, where influent constituents could be added or removed. Generally, however, effluent samples were obtained via an autosampler (Foxy® 200 fractionator), programmed to collect samples at appropriate intervals. Flow through the fracture was controlled using a peristaltic pump.

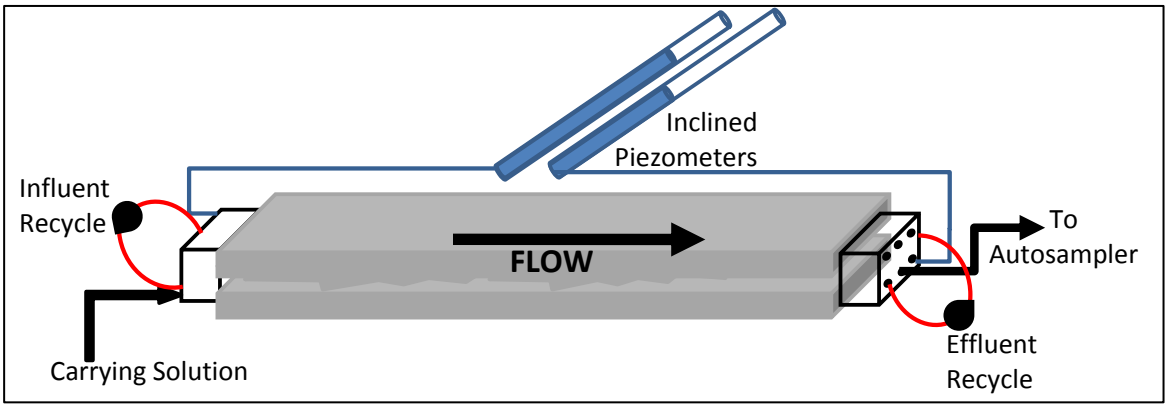

Figure 3 – Schematic diagram of the experimental apparatus

Prior to conducting experiments, each fracture was flushed with carbon dioxide and then saturated with degassed phosphate buffer solution (PBS). This promoted gas dissolution and ensured complete aqueous phase saturation of the aperture. Bromide tracer experiments were carried out at specific discharges of 5, 15, and 30 m/day to characterize the aperture field of each fracture. At each flow rate, the tracer test was carried out until effluent bromide concentrations were observed to be negligible. A high performance liquid chromatograph (HPLC) machine using an anion separation column (Hamilton PRP X-110) and hydroxybenzoic acid eluent, run at 1.8 mL/min, was used to quantify the bromide concentration in each sample. This was used in combination with a sulphuric acid regenerant run at 5 mL/min. The concentration of the regenerant was optimized to produce the best signal possible. A sample loop size of 100 µL

was used. Samples were run in triplicate and error around each measurement was estimated as three standard deviations from these measurements.

Particulate materials used for this work included *E. coli*, MS2, and 2 sizes of carboxylated microspheres (0.0425 µm and 0.525 µm). All particulate experiments were carried out at a specific discharge of approximately 15 m/day. Particulate experiments were carried out over 4 days, with changes in solution conductivity occurring after 2 days. For the first 2 days, carrying solution conductivity was 1100 ±100 µS/cm. The carrying solution was then changed and the remaining two days of the experiment were run at 98 ±15 µS/cm. Both solute and particulate materials were added to the system using the upstream sampling vial.

3.2.2 Fracture Characteristics

Fractures were characterized by their equivalent aperture across the fracture field. Tsang, (1992) clarified the different methods by which an aperture can be characterized. Briefly, three equivalent apertures can be calculated: the cubic law aperture (b_c), the mass balance aperture (b_m) and the frictional loss aperture (b_f). Equations (29), (30), and (31) below show the cubic law, mass balance and frictional loss aperture equations respectively:

$$b_c = \left(\frac{12\mu QL}{\rho g W \Delta h}\right)^{\frac{1}{3}} \tag{29}$$

$$b_m = \frac{Q\tau}{LW} \tag{30}$$

$$b_f = L\left(\frac{12\mu}{\rho g(\Delta h)\tau}\right)^{\frac{1}{2}} \tag{31}$$

where Q is the volumetric flow rate (m^3/s), L is the length of fracture (m), μ is the dynamic viscosity of water (Pa·s), ρ is the density of solution (kg/m^3), g is the gravitational constant (m^2/s), W is the fracture width (m), Δh is the measured head differential across the fracture (m), and τ is the average residence time of the constituent in the fracture(s). τ was calculated using the weighted moment method, as proposed by Fahim & Wakao (1982) in combination with data from conservative bromide tracer experiments. The three estimations of fracture aperture are expected to be different, and their spread, quantified by the COVs (32), provides an estimation of the field variability (Rodrigues et al., 2013).

$$COV_s = \frac{\sigma(b_f, b_c, b_m)}{b_m} \quad (32)$$

The COV_s is a surrogate measure of the coefficient of variation of the aperture field; a COVs of zero indicates perfectly parallel plates, and a greater COVs indicates more variability within the aperture field.

3.2.3 Carboxylated Microsphere (CM) Characteristics

Two distinct sizes of CMs were used in this work. A small size (0.0425 µm) to simulate MS2 transport, and a large size (0.525 µm) to replicate *E. coli*. Specifically, the large spheres have a surface area similar to a typical *E. coli* RS2GFP bacterium with a length of 2 µm and a diameter of 0.5 µm. The small microspheres were similar in size to MS2. Both microspheres were obtained from Polysciences Inc., and were finished with a carboxylated surface to increase the negative surface charge so that they would more closely resemble that of typical biological particles. Surfaces of the microspheres were fluorescent, optimally exciting and emitting at wavelengths of 441 nm and 486 nm respectively. CMs were enumerated by measuring the fluorescence of a given sample using a fluorescence spectrophotometer (Cary Eclipse, Varian). The recorded reading was compared to a calibration curve of known concentrations and corresponding fluorescence measurements.

3.2.4 *E. coli* RS2GFP Characteristics

E. coli RS2GFP was obtained for this work from Dr. Larry Halverson from the Department of Agriculture and Biosystems Engineering at Iowa State University via the laboratory of Dr. Emelko in the Department of Civil Engineering at the University of Waterloo. This particular strain contains a fluorescent protein and a resistance to two specific antibiotics (kanamycin and rifampicin). Enumeration was carried out by a plating method, which involved spreading 0.1 mL of sample across agar within a prepared plate, allowing to dry, inverting the plate and incubating at 37°C for approximately 20 hours. After this time, the bacterial colonies on each plate could be counted. Further details on this method are provided by Passmore et al., (2010). Error quantification considered a variety of sources, including variable source concentration, estimated error from plating, and colony counting error, and was quantified using the methodology described by Emelko, et al., (2010a, 2010b).

Stock bacteria were stored at -80°C in a solution of Luria-Bertani (LB) broth, with adequate antibiotic solutions and 10% glycerol. To prepare the experimental bacterial solutions, stock solutions were grown into the stationary growth phase. From this, one millilitre of bacteria was added to 100 mL of LB broth containing 10 µg/mL of rifampicin and 100 µg/L of kanamycin. This was grown at 36°C for approximately four hours, until optical density measurements of the growth solution ranged from 0.5-0.8. This indicated the bacteria were in the exponential growth stage. Simultaneous to each test, the decay of the *E. coli* at the given test conditions was measured twice daily through enumeration as described above. Decay was fitted to a first order decay curve, and adjustments were made to both inlet and outlet concentrations to reflect true concentrations.

3.2.5 MS2 Characteristics

Bacteriophage MS2 used for this work was obtained from Dr. Monica Emelko at the University of Waterloo, department of Civil Engineering. Generally, MS2 is a 20-25 nm icosahedral shaped coliphage. Enumeration was carried out according to the double agar overlay technique, as described by Adams, (1959) and optimized by Mesquita, (2011) for this particular strain. The host bacterium was *E. coli* ATCC 15597, also obtained from the University of Waterloo. 0.2 mL of MS2 sample was added to 0.1 mL of host and 0.1 mL of a calcium chloride/glucose solution in a separate holding container. This mixture was allowed to sit for three minutes to promote infection. Five millilitres of agar overlay was then added to this container, and the entire mixture was plated. After allowing the plate to dry, it was inverted and incubated for 12-20 hours. Plaques formed during the incubation period were enumerated. Error was estimated again using the methodology as described by Emelko et al., (2010a, 2010b). Simultaneous to each test, the MS2 concentration of stock solution was monitored through enumeration as described above. It was found that there was no significant die off over the course of each test.

3.2.6 Extended DLVO Theory

The extended DLVO theory attempts to explain interaction behaviour that has been observed, but is not currently explained by the common DLVO theory presented above. This is usually accomplished using colloid hydrophobicity to explain additional attractive and repulsive forces (Grasso et al., 2002; Redman et al., 2004; Syngouna & Chrysikopoulos, 2013; Tufenkji,

2007). Grasso et al. (2002) also suggested that Lewis acid/base interactions can be used to quantify hydrophobic forces that are related to hydrogen bonding within the fluid. It is expected that both the dolomite fracture (Géber & Gömze, 2009) and the biological material used through this investigation (Rodrigues, 2012; Syngouna & Chrysikopoulos, 2013) are hydrophobic in nature, suggesting these forces may also account for particulate adhesion and retention. However, Lewis acid/base surface potentials are not readily available. Therefore, the extended DLVO theory was not considered for this work, but represents an area of future consideration.

3.2.7 Zeta Potential

The surface properties of each particle were characterized by electrophoretic mobility, which was measured directly by a zeta analyzer. The Smoluchowski approximation was then used to calculate the zeta potential of the particle, which is an approximation of surface charge. The data are summarized in Table 1, together with zeta potentials obtained from the literature. The zeta potentials calculated in this work generally agree with those obtained from the literature. It is expected that the zeta potential will be slightly affected by the fact that ionic strength of the carrying solution decreased over the course of each experiment. The relationship between ionic strength and zeta potential is not adequately captured by the table below because of the varying particles, particle sizes and ion valences in solution.

Table 1 - Summary of zeta potential calculations for particulates used in this work

Material	Zeta Potential (mV)	Ionic Strength (mM/L)	Source
MS2	-11.7 ±3.7	66 as Na^+/K^+	This work
	-10 to -15	5 as Ca_2Cl	(Tong, Shen, Yang, & Kim, 2012)
	-15	10 as NaCl	(Harvey & Ryan, 2004)
E. coli	-12.1 ±0.7	100 as KCl	(Passmore et al., 2010)
Microspheres (0.525 µm)	-27.8 ±3.6	0.36 as Na^+/K^+	This Work
Microspheres (0.0425 µm)	-38.8 ±2.8	29 as Na^+/K^+	This Work
Microspheres (0.02 µm)	-20 to -38	3-12 as Na^+/Ca^{2+}	(Mondal & Sleep, 2013)
Microspheres (0.2 µm)	-25 to -50	3-12 as Na^+/Ca^{2+}	(Mondal & Sleep, 2013)
Microspheres (1.5 µm)	-18 ± 2	100 as KCl	(Passmore et al., 2010)
Microspheres (4.87 µm)	-38 ± 3	100 as KCl	(Passmore et al., 2010)
Microspheres (5 µm)	-18.7	10	(Harvey et al., 2008)

3.3 Experimental Results

3.3.1 Hydraulic Experiments

The relationship between specific discharge and head loss was found to be linear across all flow rates tested, as shown in Figure 4. Therefore, the flow is laminar, although it is likely that local areas of turbulence exist due to aperture field variability. Reynolds numbers, over the flow rates examined, ranged from 0.03 to 0.17. The cubic law aperture calculated from these measurements was found to be 425 µm and 499 µm for Fractures 1 and 2 respectively, which is within the range of those reported in literature (Quinn, et al., 2011c). The error associated with each measurement was estimated, and propagation of error was used to estimate error in the aperture calculations.

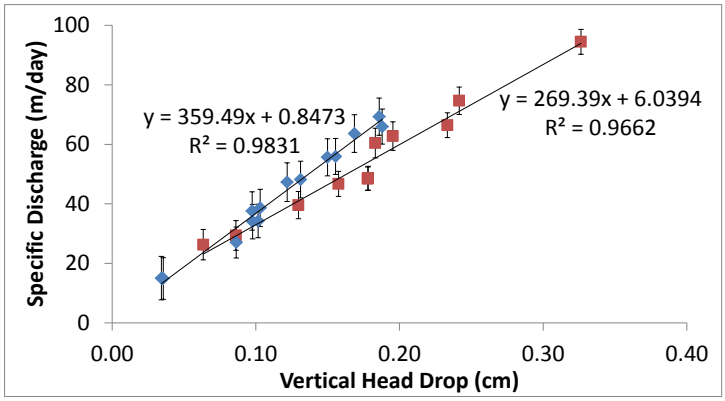

Figure 4 - Specific Discharge vs Vertical Head Drop for Fracture 1 (■) and Fracture 2 (◆).
Error bars calculated using the propagation of error for all measurement.

3.3.2 Bromide Tracer Experiments

Solute tracer experiments were conducted at three different specific discharges (5, 15 and 30 m/day), and in duplicate for the two slowest experiments to observe the repeatability of the test. Influent and effluent concentration profiles for the experiment conducted at 15 m/day in Fractures 1 and 2 are shown in Figure 5, and are typical of those from all specific discharges. A summary of the results from all tracer experiments is included in Table 2, and were used to calculate b_m and b_f according to equations (30) and (31) respectively. A summary of all aperture calculations, including the COVs, is included in Table 3. The mass recovery from all solute tracer experiments ranged from 82 – 100%.

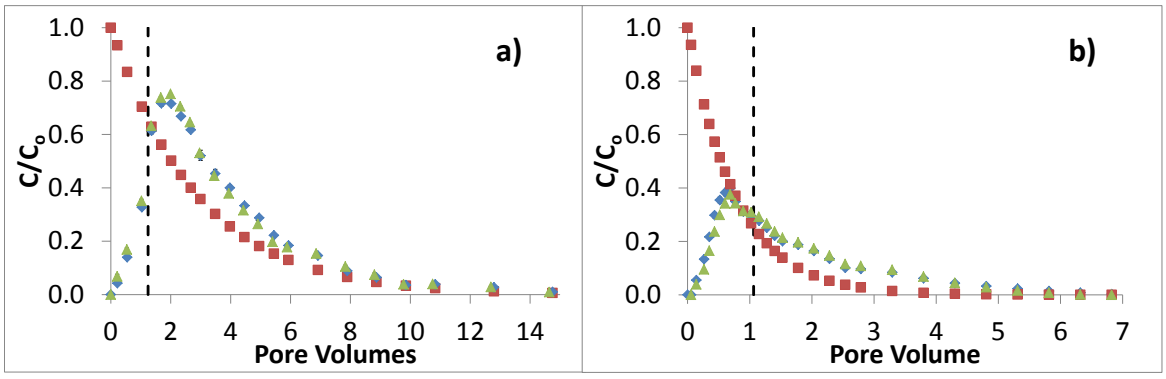

Figure 5 – Bromide tracer results from a) Fracture 1 and b) Fracture 2 at 15 m/day.
Figure shows inlet concentration (■), and effluent concentration profiles for replicate experiments 1 (◆) and 2 (▲).
Average residence time calculated by the weighted moment method is shown by the hatched line.

Table 2 - Summary of all bromide tracer test results

	Average Residence Time (min)		Recovery	
Fracture 1 – 30 m/day	34.1	±4.8	82.8%	±7.0%
Fracture 1 – 15 m/day (1)	70.9	±4.0	101.4%	±4.0%
Fracture 1 – 15 m/day (2)	70.4	±4.7	101.9%	±1.9%
Fracture 1 – 5 m/day (1)	108.8	±5.0	82.9%	±2.5%
Fracture 1 – 5 m/day (2)	116.3	±3.0	92.6%	±4.0%
Fracture 2 – 30 m/day	126.2	±4.3	92.0%	±4.7%
Fracture 2 – 15 m/day (1)	261.0	±4.7	93.6%	±3.4%
Fracture 2 – 15 m/day (2)	261.9	±5.4	93.1%	±3.6%
Fracture 2 – 5 m/day (1)	493.1	±7.8	93.3%	±6.7%
Fracture 2 – 5 m/day (2)	586.4	±7.8	98.3%	±4.7%

Table 3 - Summary of aperture calculations for both Fracture 1 and Fracture 2

	b_c (mm)		b_m (mm)		b_l (mm)		COVs
Fracture 1	0.43	±0.05	0.70	±0.09	0.33	±0.02	0.27
Fracture 2	0.50	±0.06	2.74	±0.27	0.22	±0.01	0.50

It is clear that Fracture 1 and Fracture 2, which are both dolostone rocks from different geological formations, have significantly different aperture field characteristics. Fracture 1, with a COVs of 0.27, has a (statistically significantly) less variable aperture field than Fracture 2 with a COVs of 0.5. This was expected after visual inspection of the aperture field, in which large vugs on the order of several millimeters were apparent in Fracture 2, while not immediately visible in Fracture 1.

3.3.3 Electrostatic Interactions

In this experimental work, the conductivity of the solution was altered mid test in attempt to elute any particles retained within the fracture, and evaluate the ability of the DLVO theory to predict particle-fracture interactions. Solution conductivities were measured and correlated to ionic strengths using the Marion-Babcock relationship, which was found to be an adequate method to predict ionic strengths given low conductivity soil solutions (Essington, 2004). The calculated ionic strengths used under high and low ionic strength testing conditions are summarized in Table 4.

Table 4 – Calculated stream ionic strengths

	Ionic Strength (mmol/L)
High Ionic Strength	1.38 ± 0.22
Low Ionic Strength	15.88 ± 1.46

It is important to note that some assumptions were required for the estimation of DLVO profiles related to this work. Exact values for the Hamaker constant between the particle and dolomite surface were not readily available and therefore had to be assumed. Hamaker constants including MS2 have been reported between the $4x10^{-21}$ J and $6.6x10^{-21}$ J for MS2-water-silica and MS2-water-sand systems (Anders & Chrysikopoulos, 2005; Keller et al., 2004; Sadeghi, 2012; Walker et al., 2004). Mondal & Sleep (2013) used a Hamaker constant of $6.0x10^{-21}$ J for a similar PRD1-water-dolomite rock system. Walker et al. (2004) used a value of $6.5x10^{-21}$ J for an *E. coli*-water-quartz system. Taking these sources into consideration, a Hamaker constant of $6.0x10^{-21}$ J was assumed for the MS2-water-dolomite rock system. Alternatively, Li & Logan, (2004), proposed that the Hamaker constant could be calculated according to (33).

$$H = -12\pi h_o^2 \Delta G_{ho}^{LW} \tag{33}$$

where h_o is the minimum separation distance (m), and ΔG^{LW} is the interaction energy per unit area between the bacteria and fracture surface (J/m^2). This can be approximated as follows:

$$\Delta G_{ho}^{LW} = \left(\sqrt{\gamma_w^{LW}} - \sqrt{\gamma_s^{LW}}\right)\left(\sqrt{\gamma_b^{LW}} - \sqrt{\gamma_w^{LW}}\right) \tag{34}$$

where γ_w, γ_b, γ_s are the surface tensions of the water, bacteria and fracture respectively (J/m^2). Surface tension measurements for dolomite and several strains of *E. coli* have been completed by Morrow et al., (2005). Although *E. coli* strain ATCC 15597 was not among those measured, there was little variation in the strains actually measured (32.3 – 33.2 mJ/m^2). A surface tension of 33.2 mJ/m^2 was assumed for this work resulting in a calculated Hamaker constant of $9.4x10^{-21}$ J for an *E. coli*-water-dolomite system. For the microsphere-water-rock system, a Hamaker constant of $6.4x10^{-21}$ J was assumed based on measurements provided in literature (Mondal & Sleep, 2013).

These assumptions, together with the calculated zeta potentials were used to generate energy profiles using (27) and (28), which are shown in Figure 6. The depth of the secondary energy minimum and size of energy barrier to the primary well are positively related to particle

size. The effect of reducing the conductivity of the carrying solution is shown in Figure 7 for the large microsphere system. The energy profiles change drastically under the reduced conductivity conditions, as the secondary energy minimum disappears in all three particle-fracture systems.

In general, a net negative energy indicates favourable attachment conditions, and the slope of the energy curve predicts the forces acting upon the particle at that point. At the secondary energy minimum, the force acting upon the particle is zero, indicating potential retention at this distance from the fracture. The energy profiles for all experimental particles reveal an energy barrier (large net positive energy) between the primary and secondary energy minima under the high conductivity conditions. Particles that overcome this energy barrier are generally considered irreversibly attached. Retention within the secondary energy minimum is reversible, however, as altering the conductivity of the carrying solution leads to the disappearance of this minimum. When this minimum disappears, any particles retained within the secondary minimum are eluted. Therefore, the significance of the secondary energy minimum can be determined through quantifying the number of particles eluted when the conductivity of the carrying solution is reduced.

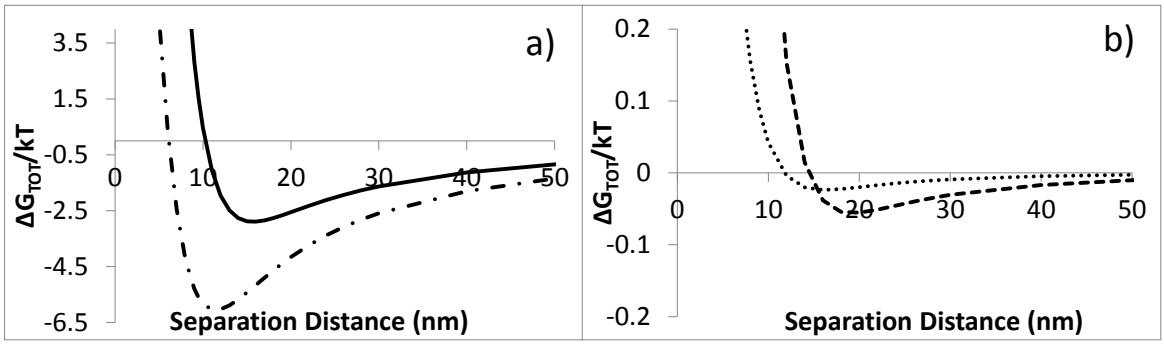

Figure 6 – Predicted DLVO energy profiles, scaled by Boltzmann`s constant (k) and temperature (T) for all particles. a) shows E. coli (– · – · – · –) and large microspheres (————) and b) shows MS2 (·····) and small microspheres (– – – –)

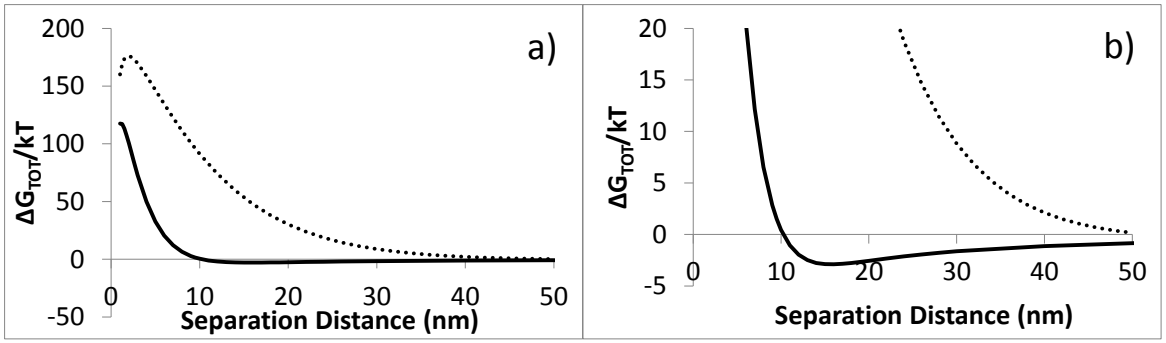

Figure 7 – DLVO energy profiles, scaled by Boltzmann`s constant (k) and temperature (T), showing effects of ionic strength of testing conditions on interaction energies.
a) shows detail for large microspheres at high (———) and low (·····) conductivities and b) shows the secondary minima at a larger scale.

3.3.4 Large Microsphere Experiments

All particulate tracer experiments were carried out at an identical specific discharge rate of 15 m/day. Figure 8 presents the results for both large microsphere experiments conducted in Fractures 1 and 2. Results are shown only from the portion of the test conducted with the high conductivity carrying solution, as significant elution was not observed when the conductivity was reduced. The mean residence time was determined using the weighted moment method (Fahim & Wakao, 1982), and is represented by the hatched line. The reproducibility between repeat experiments conducted in the same fracture is immediately observable, and is likely due, in part, to the uniform nature of microsphere surface characteristics. The mean residence time is significantly larger in Fracture 2, which has large vugs and greater variability. However, the average number of pore volumes required to flush particles from the fracture (APV) was greater for Fracture 1 even though Fracture 1 is less variable and has a smaller equivalent aperture than Fracture 2. Reduction in carrying solution conductivity from approximately 1050 µS/cm to 90 µS/cm resulted in the elution of an additional 0.5% of the large microspheres in Fracture 1. However, recovery in Fracture 2 was approaching 100% before the conductivity was reduced, and therefore the conductivity of the carrying solution did not have a measureable effect on microsphere recovery.

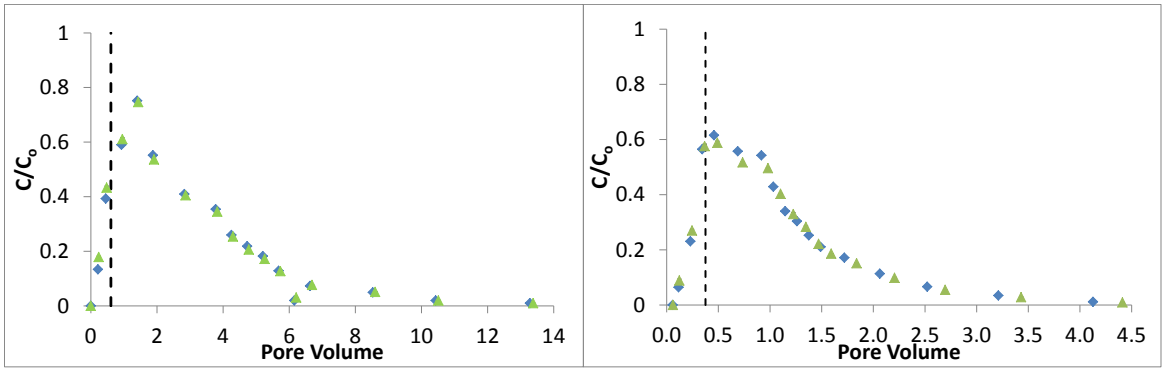

Figure 8 – Effluent concentration curves for large microspheres in a) Fracture 1 and b) Fracture 2. Experiments were conducted in duplicate (experiment 1 (▲) and experiment 2 (◆)). Hatched lines indicate the APV. Experiments were conducted at 21°C and a specific discharge of 15 m/day.

3.3.5 Small Microsphere Experiments

Effluent concentration profiles for small microspheres passed through each fracture are shown in Figure 9. Similar to the large microsphere experiments, Fracture 1 resulted in a faster mean residence time relative to Fracture 2, and recovery was higher for Fracture 2 (86.1%) relative to Fracture 1 (81.8%). Also analogous to the large microsphere experiments is that the APVs required to flush the small microspheres out of the fracture was greater for Fracture 1 than Fracture 2. Reducing the conductivity of the carrying solution resulted in the elution of 0.6% and 0.3% more microspheres for Fractures 1 and 2 respectively. Residence time for small particles was significantly longer than for larger ones, likely due to increased diffusion through the fracture plane. Increased diffusion would cause the smaller particle to move closer to the fracture wall, where flow is slower, or into low flow areas of the fracture. In general, the microsphere experiments revealed the presence of the secondary energy minimum, as predicted by DLVO theory, through the elution of additional microspheres when the conductivity of the carrying solution was reduced. However, this retention mechanism proved to be very small (<1%) relative to the overall retention in both fractures

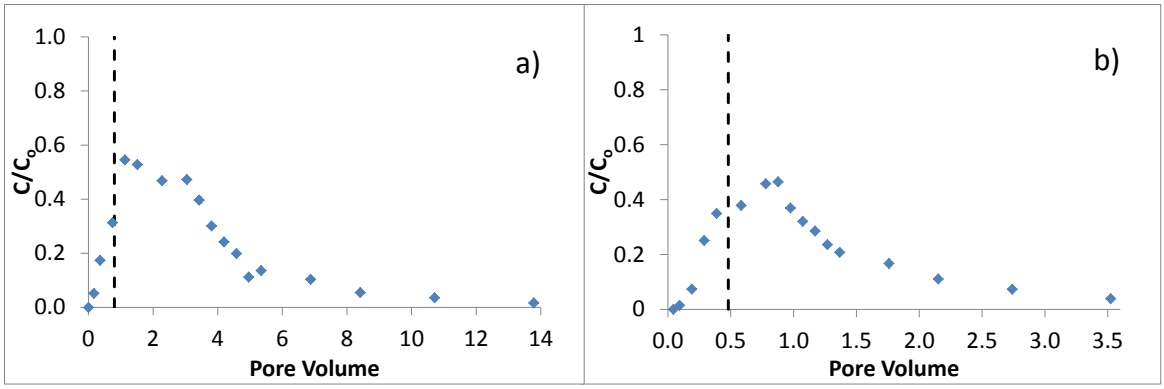

Figure 9 – Effluent concentration curves for small microspheres through a) Fracture 1 and b) Fracture 2 Figures show experimental results (◆) and mean residence time (vertical hatched line). Experiments conducted at 21°C and a specific discharge of 15 m/day.

3.3.6 MS2 Experiments

Effluent concentration profiles for the MS2 experiments in Fractures 1 and 2 are shown in Figure 10. The average residence time between duplicate experiments are significant, but can be attributed to inherent differences within biological populations (Bolster et. al, 2000). Between Fractures 1 and 2, MS2 recovery was similar but the mean residence times were significantly different. In two of the MS2 experiments, reducing the conductivity of the carrying solution resulted in elution of MS2. However, the amount eluted was negligible relative to the total recovery (<0.1%). Therefore, while this work suggests that the secondary energy minimum will work to retain particles, it is relatively insignificant to other, less reversible retention mechanisms. Analogous to the microsphere experiments, a larger number of pore volumes were required to flush the MS2 from the Fracture 1 relative to Fracture 2, even though the mean residence time was larger in Fracture 2 due to its larger variability and equivalent aperture.

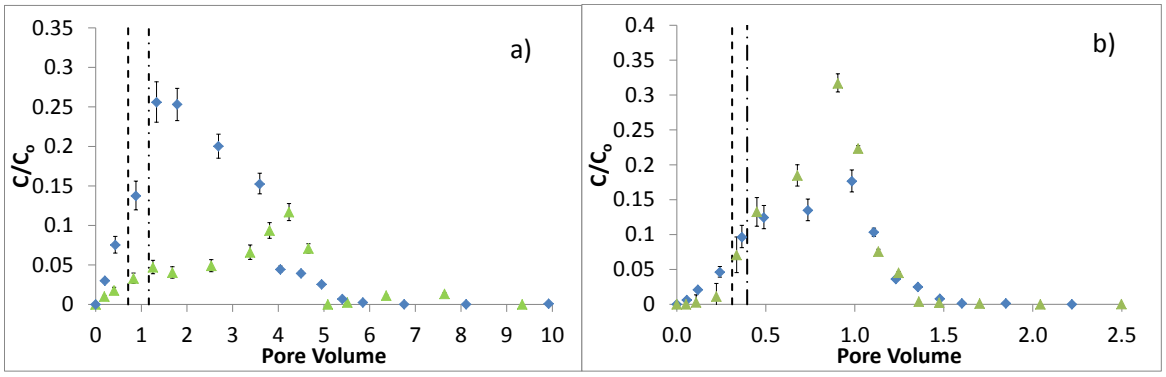

Figure 10 – Duplicate effluent concentration profiles for MS2 through a) Fracture 1 and b) Fracture 2. Mean residence times shown by the hatched lines for experiment 1 (▲, – – –) and experiment 2 (◆, —— · ——). Experiments conducted at 21°C and a specific discharge of 15 m/day.

3.3.7 *E. coli* Bacteria Experiments

The effluent concentration profiles for Fractures 1 and 2 are shown in Figure 11. The smaller, less variable Fracture 1 transports particles much faster than Fracture 2, as evidenced by their average residence times of 32.6 minutes and 98.4 minutes respectively. However, it takes a larger number of pore volumes to facilitate this transport in Fracture 1 as the average number of pore volumes required to remove the particles from the fracture was 0.517 and 0.376 for Fractures 1 and 2 respectively. Further, less *E. coli* dispersion was observed in Fracture 1 relative to Fracture 2. Changing the carrying solution mid experiment did not result in the elution of any additional bacteria in either fracture. A summary of the residence time and recovery for all particulate tracer experiments is included in Table 5.

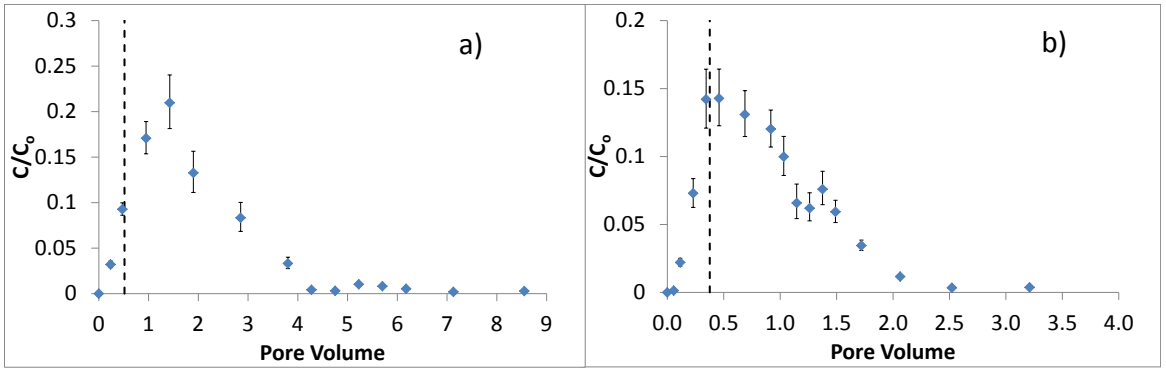

Figure 11 – Effluent concentration curves for *E. coli* through a) Fracture 1 and b) Fracture 2. The figure shows experimental results (◆) and average residence time (hatched). Experiments conducted at 21°C and a specific discharge of 15 m/day.

Table 5 - Summary of results for all particulate experiments. Experiments conducted at 21°C and a specific discharge of 15 m/day.

	Mean Residence Time (Pore Volumes)		Percent Recovery		No. of Particles
	Fracture 1	**Fracture 2**	**Fracture 1**	**Fracture 2**	
MS2	0.713 ±0.071	0.311 ±0.022	24.6 ±2.2	16.6 ±2.0	2.12×10^{9} PFUs
MS2 (repeat)	1.165 ±0.036	0.395 ±0.018	10.4 ±1.4	21.5 ±1.8	2.38×10^{9} PFUs
SM Microsphere	0.802 ±0.023	0.481 ±0.007	81.8 ±1.7	85.9 ±1.3	6.02×10^{14} particles
E. coli	0.517 ±0.075	0.376 ±0.013	17.6 ±2.5	27.9 ±3.9	2.46×10^{9} CFUs
LRG Microsphere	0.586 ±0.089	0.376 ±0.017	84.8 ±1.2	99.8 ±1.4	3.28×10^{11} particles
LRG Microsphere (repeat)	0.605 ±0.091	0.337 ±0.021	84.1 ±1.1	100.4 ±0.9	3.28×10^{11} particles

3.4 Discussion

3.4.1 Aperture Characterization

The solute tracer experiments revealed quantifiable differences between the aperture fields of Fractures 1 and 2. Generally, μ_m values indicate that Fracture 2 has a larger mean aperture than Fracture 1, and the COVs indicate that while both fractures have variable aperture fields, Fracture 2 is significantly more variable than Fracture 1. Although the hydraulic experiments and Reynolds numbers indicated that these experiments were conducted in the laminar flow regime, it is important to note that local regions of turbulence likely existed during all experiments due to the variability of these aperture fields (Cardenas et al., 2007). Particles can be delayed or retained within these turbulent areas, resulting in significantly slower travel times. Conversely, entry into these turbulent areas can be difficult for larger particles, effectively decreasing the mean aperture, forcing particles into the higher velocity part of the profile, resulting in faster transport times.

3.4.2 Effects of Aperture Field on Particulate Transport

Differences in the aperture fields between fractures resulted in significantly different transport characteristics. In both fractures, at the same specific discharge, particles in Fracture 2 had a shorter APV and were subject to longer tails. Given the no-slip assumption employed at the fracture surface, a larger aperture allows for greater stream velocities, as predicted by the parabolic velocity profile. Further, the increased COVs observed in Fracture 2 led to the development of local eddies, isolating some low flow areas of the fracture from particle transport. Similarly, particles were excluded from extreme low velocity regions near the fracture surface due to their size. All of these factors led to the shorter APV observed in Fracture 2 relative to Fracture 1.

Within the same fracture, larger particles generally had faster residence times, as described by the APV. Smaller particles, which have larger diffusion coefficients, were able to travel through a larger portion of the fracture, thereby slowing their transport.

For identical particles, recovery was generally greater in Fracture 2 than Fracture 1. These findings agree with those of Mondal & Sleep, (2012), and suggest that fewer particle/fracture interactions occurred in Fracture 2, resulting in increased recovery. It is likely that the larger COVs of Fracture 2 led to more areas of local turbulence, which act as a boundary preventing particles with lower diffusion coefficients (i.e. larger particles) from contacting the fracture walls, leading to higher recoveries. This postulation is further supported by the slightly lower recoveries of smaller CMs relative to larger CMs, in both fractures, as their larger diffusion coefficients may enable diffusion into some of these eddies. These findings suggest that smaller less variable apertures, with fewer zones of localized turbulence, lead to increased particle/wall interactions thereby increasing particle retention within the fracture. This has implications in well fields, as increased fluid velocity, induced by pumping, can result in less removal of particle contaminants.

3.4.3 Effects of Particle Surface Characteristics and Size

In general, smaller particles experienced larger residence times in both fractures. Their larger diffusion coefficients together with the fact that they experience less size exclusion enable them to enter lower flow areas of the fracture and therefore have smaller average velocities. This observation did not hold perfectly for Fracture 2, as there were no significant differences in

transport times between large CMs, *E. coli* and MS2. Fracture 2 is more variable, and therefore local areas of turbulence and increased hydrodynamic forces are more likely. As stated above, particles are precluded from entering these zones unless they have large diffusion coefficients. Therefore, it is likely that the range of velocities that the different sized particles were able to sample was similar, resulting in similar travel times. The increased APV observed for small microspheres in Fracture 2 is likely in part due to its increased diffusion coefficient relative to larger particles.

These experiments also highlight the importance of surface properties on particle transport and retention. The energy profiles in Figure 6 show that at initial ionic strengths a secondary energy minimum exists for all particles employed in these experiments. This secondary minimum disappears when the ionic strength of the solution drops, as done in this work. The depth of this secondary energy minimum is positively related to the particle's size and inversely related to its zeta potential. Altering solution conductivity elicited a small degree of elution for most particle types, with the exception of *E. coli*, ranging from 0-1%. This response was not consistent between experiments. Therefore, it was determined that while the secondary energy minimum is a valid mechanism for particulate retention, it is almost insignificant at the ionic strengths employed in these experiments. This is supported by the results of Mondal & Sleep (2012), who passed three different sizes of microspheres through a dolomite fracture until the effluent concentration was constant. They then decreased the ionic strength of the carrying solution to encourage microsphere elution. While their findings support the presence of secondary energy minimum, elution of particles ranged from negligible to 4% depending on the size of microsphere. A similar study was completed in porous media using fluorescent CMs by Nocito-Gobel & Tobiason, (1996). While they were also able to elute some microspheres from the porous media by changing the ionic strength of solution, percentage of particles eluted ranged drastically and depended strongly on the initial strength of carrying solution, and the number of particles initially deposited. Overall, they recorded elution between 0% and 10%, with many observations near the 0-1% range.

The DLVO theory has been used extensively to explain the deposition of biological material on fractured (Mondal & Sleep, 2013) and porous media (Redman et al., 2004; Tong et al., 2012; Tufenkji, 2007; Tufenkji & Elimelech, 2004; Walker et al., 2004). These sources

conclude that biological material tends to agree with historical DLVO conclusions (i.e., increased retention under increased ionic strength conditions); however, significant deviations from the DLVO theory have been observed (mainly the retention of biological material in the presence of predicted unfavourable attachment conditions). This work observed significantly more retention of biological particulate material relative to CMs, even though predicted energy profiles for all materials show the existence of similar secondary energy minima. These energy minima were found to be a negligible retention mechanism when considering either biological or microsphere transport through dolomite fractures under these ionic strength conditions. Between CMs and biological particulates of similar surface area, transport time was similar, but recovery was not. The inability of CMs to replicate a key transport indicator (recovery) confirms significant transport differences between biological particles and CMs, leading to the conclusion that CMs are poor surrogates for modelling biological particle recovery in fractures. It has been suggested that surface properties and heterogeneities of biological material will affect certain measurements taken, such as electrophoretic mobility measurements (Langlet et al., 2008). This work demonstrates that the surface properties of biological particulates also affect adhesion and retention of particles in fractured media, and therefore characterization of biological material and prediction of particle transport using electrophoretic mobility measurements may not be appropriate. However, the application for which CMs are to be used must be considered. If CMs are only required to emulate the transport time of biological particles, their use may be appropriate.

The colloid filtration theory (CFT) has often been used to describe the transport of particles through porous media (Tufenkji, 2007; Tufenkji & Elimelech, 2004), and has recently been extended to fractured media (Mondal & Sleep, 2013). Three different retention mechanisms are accounted for by this theory: diffusion, interception and sedimentation (Foppen & Schijven, 2006). However, it has been well documented by Tufenkji, (2007) and Tufenkji & Elimelech (2004, 2005), that CFT breaks down under unfavourable attachment conditions due to the surface heterogeneities of biological cells. This work confirms that cell transport is much different than that of similar CMs, and an adequate model to describe their transport through fractures has thus far been elusive.

4.0 Conclusions

This work clarified several mechanisms of particle transport within single, saturated rock fractures through varying the type of tracer and the ionic strength of the carrying solution. Detailed results from this work have given rise to the following conclusions:

- Hydraulic experiments show a linear relationship between specific discharge and head drop across the fracture. Reynolds numbers across all experiments were quite small, ranging from 0.03 to 0.17. Therefore, flow is generally expected to be linear within the fracture, although it is known that local eddying and areas of turbulence will exist.

- The APV required for particle elution for Fracture 2 is less than that required for Fracture 1. This trend is more pronounced with particulate material relative to tracers. Diffusion and size exclusion of particulate material controls the region of the fracture available for transport, and results in reduced APV for Fracture 2

- The largest particles (*E. coli* and large carboxylated microspheres) were transported the quickest, followed by small particles (MS2 and small carboxylated microspheres), with the slowest being bromide ions. Increased diffusion coefficients of smaller particles allow for entry into low flow areas, including local turbulent areas (eddies).

- Increased average aperture and aperture variability led to increased recovery of carboxylated microspheres as well. This suggests that increased variability also leads to increased channelling and size exclusion, reducing the interaction between particle and fracture wall. Channelling is potentially a side effect of local eddying, making certain volumes of the fracture unavailable for particulate transport, depending on the diffusion coefficient.

- Comparison between two similarly sized particles with different surface characteristics (biological vs. non-biological) indicated surface properties are very important. Although estimated energy profiles were similar, retention was much larger for biological

particles, even after correcting for die off. This confirms the importance of surface charge heterogeneity and the 'soft' biological surface on particulate retention.

- It was shown that carboxylated microspheres are a poor surrogate for examining the retention of biological particulates with similar surface areas in fractures. This is likely due to differences in surface characteristics and subsequent interactions with the fracture wall.

- Carboxylated microspheres were shown to be an acceptable surrogate for measuring particle transport time. Therefore, depending on the parameter that is trying to be replicated (transport time or retention), carboxylated microspheres may be an adequate model biological particles.

- Alteration of the carrying solution ionic strength resulted in negligible elution of additional biological or non-biological particulate material. Therefore, although estimated energy profiles predicted the presence of secondary energy minima, this proved to be a relatively insignificant retention mechanism.

- This work further supports the ineffectiveness of colloid filtration theory to explain the movement of biological particulate material through fractures. This is accentuated by the differences in retention between similarly sized particles with similar energy profiles. These differences are unexplained by current filtration or DLVO theories, and suggest that an adequate model to predict particulate transport through fractured material does not currently exist.

Recommendations

- Carry out similar experiments with additional biological material to evaluate the repeatability of biological adhesion within a fractured setting.

- Attempt to evaluate electrostatic parameters more accurately, such as Hamaker constants between particulate material and dolostone fractures, and surface charge heterogeneities of biological material.

- Further work could be carried out on additional fractures of many different characteristics to determine if the results observed here with respect to fracture variability and recovery are repeatable. Additionally, a small scaling up to consider particulate transport through a small number of fractures. This would be a link between laboratory and field work, and serve to comment on the overall governing mechanisms of transport. I.e., although important on a local scale, the mechanisms suggested here may be inconsequential within a fractured rock network. Alternatively, diffusive and channelling mechanisms may be accentuated in a fracture network, amplifying the observations noted here in a single fracture.

- Further examination of biological transport accompanied by a representative food source should be considered. This may significantly alter transport conditions, and therefore change the perceptions of biological transport.

References

Abdel-Salam, A., & Chrysikopoulos, C. V. (1995). Modeling of Colloid and Colloid-Facilitated Contaminant Transport in a Two-Dimensional Fracture with Spatially Variable Aperture. *Transport in Porous Media*, 197–221.

Adams, M. H. (1959). *Bacteriophages*. New York: Interscience Publishers Inc.

Anders, R., & Chrysikopoulos, C. V. (2005). Virus fate and transport during artificial recharge with recycled water. *Water Resources Research*, *41*(10).

Anderssen, a. S., & White, E. T. (1971). Parameter estimation by the weighted moments method. *Chemical Engineering Science*, *26*(8), 1203–1221. doi:10.1016/0009-2509(71)87007-0

Bakker, D. P., Busscher, H. J., & van der Mei, H. C. (2002). Bacterial Deposition in a Parallel Plate and Stagnation Point Flow Chamber. *Microbiology*, *148*, 597–603.

Bauget, F., & Fourar, M. (2008). Non-Fickian dispersion in a single fracture. *Journal of contaminant hydrology*, *100*(3-4), 137–48. doi:10.1016/j.jconhyd.2008.06.005

Bear, J., Tsang, C.-F., & de Marsily, G. (1993). *Flow and Contaminant Transport in Fractured Rock*. Academic Press Inc.

Becker, M. W., Metge, D. W., Collins, S. a, Shapiro, A. M., & Harvey, R. W. (2003). Bacterial transport experiments in fractured crystalline bedrock. *Ground water*. Ground Water. Retrieved from http://www.ncbi.nlm.nih.gov/pubmed/13678122

Berkowitz, B. (2002). Characterizing flow and transport in fractured geological media : A review. *Advances in Water Resources*, *25*, 861–884.

Bird, R. B., Stewart, W. E., & Lightfoot, E. N. (2002). *Transport Phenomena* (Second Edi.). John Wiley & Sons, Inc.

Bodin, J., Delay, F., & de Marsily, G. (2003). Solute transport in a single fracture with negligible matrix permeability: 1. fundamental mechanisms. *Hydrogeology Journal*, *11*(4), 418–433. doi:10.1007/s10040-003-0268-2

Bolster, C. H., Mills, A. L., Hornberger, G., & Herman, J. (2000). Effect of Intra-Population Variability on the Long-Distance Transport of Bacteria. *Ground Water*, *38*(3), 370–375.

Bos, R., van der Mei, H. C., & Busscher, H. J. (1999). Physico-chemistry of initial microbial adhesive interactions--its mechanisms and methods for study. *FEMS microbiology reviews*, *23*(2), 179–230. Retrieved from http://www.ncbi.nlm.nih.gov/pubmed/10234844

Boström, M., Williams, D., & Ninham, B. (2001). Specific Ion Effects: Why DLVO Theory Fails for Biology and Colloid Systems. *Physical Review Letters*, *87*(16), 1–4. doi:10.1103/PhysRevLett.87.168103

Brush, D. J., & Thomson, N. R. (2003). Fluid flow in synthetic rough-walled fractures: Navier-Stokes, Stokes, and local cubic law simulations. *Water Resources Research*, *39*(4). doi:10.1029/2002WR001346

Burke, M. G. (2012). *Exploring the effects of aperture size , aperture variability and matrix properties on biocolloid transport and retention in a single saturated fracture*. McMaster University.

Cardenas, M. B., Slottke, D. T., Ketcham, R. a., & Sharp, J. M. (2007). Navier-Stokes flow and transport simulations using real fractures shows heavy tailing due to eddies. *Geophysical Research Letters*, *34*(14), L14404. doi:10.1029/2007GL030545

Cherry, J. A., Parker, B. L., Bradbury, K. R., Eaton, T. T., Gotkowitz, M. B., & Hart, D. J. (2006). Groundwater Flow through Aquitards. In *Contaminant Transport Through Aquitards : A " State of the Science " Review* (pp. 31–62).

Chrysikopoulos, C. V., & Abdel-Salam, A. (1997). Modeling colloid transport and deposition in saturated fractures. *Colloids and Surfaces A: Physicochemical and Engineering Aspects*, *121*, 189–202.

Crittenden, J. C., Trussell, R. R., Hand, D. W., Howe, K. J., & Tchobanoglous, G. (2005). *Water Treatment Principles and Design* (Second Edi.).

Cumbie, D. H., & McKay, L. D. (1999). Influence of diameter on particle transport in a fractured shale saprolite. *Journal of Contaminant Hydrology*, *37*(1-2), 139–157. doi:10.1016/S0169-7722(98)00156-9

Darbha, G. K., Schäfer, T., Heberling, F., Lüttge, A., & Fischer, C. (2010). Retention of latex colloids on calcite as a function of surface roughness and topography. *Langmuir : the ACS journal of surfaces and colloids*, *26*(7), 4743–52. doi:10.1021/la9033595

Dehghan, M. (2004). Numerical solution of the three-dimensional advection–diffusion equation. *Applied Mathematics and Computation*, *150*(1), 5–19. doi:10.1016/S0096-3003(03)00193-0

Emelko, M. B., Schmidt, P. J., & Reilly, P. M. (2010a). Particle and microorganism enumeration data: enabling quantitative rigor and judicious interpretation. *Environmental science & technology*, *44*(5), 1720–7. doi:10.1021/es902382a

Emelko, M. B., Schmidt, P. J., & Reilly, P. M. (2010b). Particle and microorganism enumeration data: enabling quantitative rigor and judicious interpretation. *Environmental science & technology*, *44*(5), 1720–7. doi:10.1021/es902382a

Essington, M. E. (2004). *Soil and Water Chemisty: An Integrative Approach* (pp. 223–224). Boca Raton: CRC Press LLC.

Fahim, M. A., & Wakao, N. (1982). Parameter Estimation from Tracer Response Measurements. *The Chemical Engineering Journal*, *25*, 1–8.

Fetter, C. W. (1999). *Contaminant Hydrogeology* (2nd ed.). Prentice-Hall.

Figliola, R. S., & Beasley, D. E. (2006). *Theory and Design for Mechanical Measurements* (Fourth.). John Wiley & Sons, Inc.

Foppen, J. W. A., & Schijven, J. F. (2006). Evaulation of data from the literature on the transport and survival of Escherichia coli and thermotolerant coliforms in aquifers under saturated conditions. *Water Research*, *40*(3), 401–426.

Fox, R. W., Pritchard, P. J., & McDonald, A. T. (2009). *Introduction to Fluid Mechanics* (Seventh.). John Wiley & Sons, Inc.

Frazier, C. S., Graham, R. C., Shouse, P. J., Yates, M. V., & Anderson, M. a. (2002). A Field Study of Water Flow and Virus Transport in Weathered Granitic Bedrock. *Vadose Zone Journal*, *1*(1), 113–124. doi:10.2113/1.1.113

Freeze, A. R., & Cherry, J. A. (1979). *Groundwater*.

Géber, R., & Gömze, L. A. (2009). Investigation of Hydrophilic and Hydrophobic Properties of Different Mineral Fillers for Asphalt Mixtures, 945–950.

Grabow, W. (2001). Bacteriophages : Update on application as models for viruses in water. *Waer SA*, *27*(2), 251–268.

Grasso, D., Subramaniam, K., Butkus, M., Strevett, K., & Bergendahl, J. (2002). A review of non-DLVO interactions in environmental colloidal systems. *Environmental Science and Biotechnology*, 17–38.

Guan, H., Schulze-Makuch, D., Schaffer, S., & Pillai, S. (2003). The effect of critical pH on virus fate and transport in saturated porous medium. *Ground water*, *41*(5), 701–8. Retrieved from http://www.ncbi.nlm.nih.gov/pubmed/13678124

Harvey, R. W., Metge, D. W., Shapiro, A. M., Renken, R. a., Osborn, C. L., Ryan, J. N., … Landkamer, L. (2008). Pathogen and chemical transport in the karst limestone of the Biscayne aquifer: 3. Use of microspheres to estimate the transport potential of Cryptosporidium parvum oocysts. *Water Resources Research*, *44*(8), 1–12. doi:10.1029/2007WR006060

Harvey, R. W., & Ryan, J. N. (2004). Use of PRD1 bacteriophage in groundwater viral transport, inactivation, and attachment studies. *FEMS microbiology ecology*, *49*(1), 3–16. doi:10.1016/j.femsec.2003.09.015

Hoek, E. M. V, & Agarwal, G. K. (2006). Extended DLVO interactions between spherical particles and rough surfaces. *Journal of colloid and interface science*, *298*(1), 50–8. doi:10.1016/j.jcis.2005.12.031

Hrudey, S. E., Payment, P., Huck, P. M., Gillham, R. W., & Hrudey, E. J. (2003). A fatal waterborne disease epidemic in Walkerton, Ontario: comparison with other waterborne outbreaks in the developed world. *Water science and technology : a journal of the International Association on Water Pollution Research*, *47*(3), 7–14. Retrieved from http://www.ncbi.nlm.nih.gov/pubmed/12638998

James, S. C., Bilezikjian, T. K., & Chrysikopoulos, C. V. (2005). Contaminant transport in a fracture with spatially variable aperture in the presence of monodisperse and polydisperse colloids. *Stochastic Environmental Research and Risk Assessment*, *19*(4), 266–279. doi:10.1007/s00477-004-0231-3

James, S. C., & Chrysikopoulos, C. V. (2000). Transport of polydisperse colloids in a saturated fracture with spatially variable aperture. *Water Resources*, *36*(6), 1457–1465.

Keller, A. a., Sirivithayapakorn, S., & Chrysikopoulos, C. V. (2004). Early breakthrough of colloids and bacteriophage MS2 in a water-saturated sand column. *Water Resources Research*, *40*(8), n/a–n/a. doi:10.1029/2003WR002676

Koyama, T., Neretnieks, I., & Jing, L. (2008). A numerical study on differences in using Navier–Stokes and Reynolds equations for modeling the fluid flow and particle transport in single rock fractures with shear. *International Journal of Rock Mechanics and Mining Sciences*, *45*(7), 1082–1101. doi:10.1016/j.ijrmms.2007.11.006

Lakkapragada, S., & Walz, J. Y. (1996). Effect of Surface Roughness on the Interaction Energy between a Colloidal Sphere and a Flat Plate. *Journal of Colloid and Interface Science*, *183*, 199–213.

Langlet, J., Gaboriaud, F., Gantzer, C., & Duval, J. F. L. (2008). Impact of chemical and structural anisotropy on the electrophoretic mobility of spherical soft multilayer particles: the case of bacteriophage MS2. *Biophysical journal*, *94*(8), 3293–312. doi:10.1529/biophysj.107.115477

Lennox, E. S. (1955). Transduction of Linked Genetic Characters of the Host by Bacteriophage P1. *Virology*, 190–206.

Li, B., & Logan, B. E. (2004). Bacterial adhesion to glass and metal-oxide surfaces. *Colloids and surfaces. B, Biointerfaces*, *36*(2), 81–90. doi:10.1016/j.colsurfb.2004.05.006

Mckay, L., Cherry, J. A., & Bales, R. C. (1993). A Field Example of Bacteriophage as Tracers of Fracture Flow. *Environmental Science and Technology*, *27*(6), 1075–1079.

Mckay, L. D., Cherry, J. A., & Gillham, W. (1993). Field Experiments in a Fractured Clay Till 1. Hydraulic Conductivity and Fracture Aperture. *Water Resources Research*, *29*(4).

Mckay, L. D., Gillham, R. W., & Cherry, J. A. (1993). Field Experiments in a Fractured Clay Till 2. Solute and Colloid Transport. *Water Resources Research*, *29*(12), 3879–3890.

Mesquita, M. (2011). *MS2 Bacteriophage - Enumeration*. Waterloo.

Mondal, P. K., & Sleep, B. E. (2012). Colloid transport in dolomite rock fractures: effects of fracture characteristics, specific discharge, and ionic strength. *Environmental science & technology*, *46*(18), 9987–94. doi:10.1021/es301721f

Mondal, P. K., & Sleep, B. E. (2013). Virus and virus-sized microsphere transport in a dolomite rock fracture. *Water Resources Research*, *49*(January), n/a–n/a. doi:10.1002/wrcr.20086

Morrow, J. B., Stratton, R., Yang, H. H., Smets, B. F., & Grasso, D. (2005). Macro- and nanoscale observations of adhesive behavior for several E. coli strains (O157:H7 and environmental isolates) on mineral surfaces. *Environmental science & technology*, *39*(17), 6395–404. Retrieved from http://www.ncbi.nlm.nih.gov/pubmed/16190192

Munn, J. D. (2012). *High-resolution discrete fracture network characterization using inclined coreholes in a Silurian dolostone aquifer in Guelph, Ontario*. University of Guelph.

Nocito-Gobel, J., & Tobiason, J. E. (1996). Effects of ionic strength on colloid deposition and release. *Colloids and Surfaces A: Physicochemical and Engineering Aspects*, *107*, 223–231. doi:10.1016/0927-7757(95)03340-8

Novakowski, K., Bickerton, G., Lapcevic, P., Voralek, J., & Ross, N. (2006). Measurements of groundwater velocity in discrete rock fractures. *Journal of contaminant hydrology*, *82*(1-2), 44–60. doi:10.1016/j.jconhyd.2005.09.001

Odén, M., Niemi, A., Tsang, C.-F., & Öhman, J. (2008). Regional channelized transport in fractured media with matrix diffusion and linear sorption. *Water Resources Research*, *44*(2), 1–16. doi:10.1029/2006WR005632

Ohman, J., Niemi, A., & Tsang, C. (2004). *A Regional-Scale Particle-Tracking Method for Nonstationary Fractured Media*.

Ojha, C., Surampalli, R. Y., Sharma, P. K., & Joshi, N. (2011). Breakthrough Curves and Simulation of Virus Transport through Fractured Porous Media. *Journal of Environmental Engineering*, *137*(8), 731–739. doi:10.1061/(ASCE)EE.1943-7870.0000374.

Passmore, J. M., Rudolph, D. L., Mesquita, M. M. F., Cey, E. E., & Emelko, M. B. (2010). The utility of microspheres as surrogates for the transport of E. coli RS2g in partially saturated agricultural soil. *Water research*, *44*(4), 1235–45. doi:10.1016/j.watres.2009.10.010

Pehme, P. E., Parker, B. L., Cherry, J. a, & Greenhouse, J. P. (1999). Improved resolution of ambient flow through fractured rock with temperature logs. *Ground water*, *48*(2), 191–205. doi:10.1111/j.1745-6584.2009.00639.x

Qu, J. (2010). *A Comparison of Biocolloid and Colloid Transport in Single, Saturated Rock Fractures*. McMaster University.

Quinn, P., Cherry, J., & Parker, B. (2011a). Quantification of non-Darcian flow observed during packer testing in fractured sedimentary rock. *Water Resources Research*, *47*(9). doi:10.1029/2010WR009681

Quinn, P., Cherry, J., & Parker, B. (2011b). Using slug tests to confirm non-Darcian flow identified by constant head step tests in fractured rock boreholes. In *GeoHydro 2011*.

Quinn, P., Parker, B., & Cherry, J. (2011). Using constant head step tests to determine hydraulic apertures in fractured rock. *Journal of contaminant hydrology*, *126*(1-2), 85–99. doi:10.1016/j.jconhyd.2011.07.002

Redman, J., Walker, S., & Elimelech, M. (2004). Bacterial adhesion and transport in porous media: role of the secondary energy minimum. *Environmental science & technology*, *38*(6), 1777–85. Retrieved from http://www.ncbi.nlm.nih.gov/pubmed/15074689

Rodrigues, S. (2012). *Identifying the Retention Mechanisms of (Bio) Colloids in Single, Saturated, Variable- Aperture Fractures*. McMaster University.

Rodrigues, S., & Dickson, S. (2013). A Phenomenological Model for Particle Retention in Single, Saturated Fractures. *Ground water*. doi:10.1111/gwat.12062

Rodrigues, S. N., Dickson, S. E., & Qu, J. (2013). Colloid retention mechanisms in single, saturated, variable-aperture fractures. *Water research*, *47*(1), 31–42. doi:10.1016/j.watres.2012.08.033

Ryan, J. N., & Elimelech, M. (1996). Colloid mobilization and transport in groundwater. *Colloids and Surfaces A: Physicochemical and Engineering Aspects*, *107*(95), 1–56. doi:10.1016/0927-7757(95)03384-X

Sadeghi, G. (2012). *Effect of hydrochemical conditions on transport properties of viruses in groundwater*. Utrecht University.

Saleh, N., & Kim, H. (2008). Ionic Strength and Composition Affect the Mobility of in Water-Saturated Sand Columns. *Environmental Science and Technology*, 3349–3355.

Schijven, J. F., Hassanizadeh, S. M., & de Bruin, R. H. a M. (2002). Two-site kinetic modeling of bacteriophages transport through columns of saturated dune sand. *Journal of contaminant hydrology*, *57*(3-4), 259–79. Retrieved from http://www.ncbi.nlm.nih.gov/pubmed/12180812

Schutten, M. (2012). *The influence of hydrodynamic forces on the transport and retention of colloids in single, saturated, dolomitic limestone fractures*. McMaster University.

Shen, C., Wang, F., Li, B., Jin, Y., Wang, L.-P., & Huang, Y. (2012). Application of DLVO energy map to evaluate interactions between spherical colloids and rough surfaces. *Langmuir : the ACS journal of surfaces and colloids*, *28*(41), 14681–92. doi:10.1021/la303163c

Singhal, B. B. S., & Gupta, R. P. (2010). Applied Hydrogeology of Fractured Rocks. *Media*. doi:10.1007/978-90-481-8799-7

Snow, D. T. (1965). *A parallel plate model of fractured permeable media*. University of California, Berkeley.

Soni, K. a, Balasubramanian, A. K., Beskok, A., & Pillai, S. D. (2008). Zeta potential of selected bacteria in drinking water when dead, starved, or exposed to minimal and rich culture media. *Current microbiology*, *56*(1), 93–7. doi:10.1007/s00284-007-9046-z

Syngouna, V. I., & Chrysikopoulos, C. V. (2013). Cotransport of clay colloids and viruses in water saturated porous media. *Colloids and Surfaces A: Physicochemical and Engineering Aspects*, *416*, 56–65. doi:10.1016/j.colsurfa.2012.10.018

Tchobanoglous, G., Burton, F., & Stensel, D. (2003). *Wastewater Engineering Treatment and Reuse* (4th ed.). McGraw-Hill.

Tong, M., Shen, Y., Yang, H., & Kim, H. (2012). Deposition kinetics of MS2 bacteriophages on clay mineral surfaces. *Colloids and surfaces. B, Biointerfaces*, *92*, 340–7. doi:10.1016/j.colsurfb.2011.12.017

Tsang, Y. W. (1992). Usage of "Equivalent Apertures" for Rock Fractures as Derived From Hydraulic and Tracer Tests. *Water Resources Research*, *28*(5), 1451–1455.

Tufenkji, N. (2007). Modeling microbial transport in porous media: Traditional approaches and recent developments. *Advances in Water Resources*, *30*(6-7), 1455–1469. doi:10.1016/j.advwatres.2006.05.014

Tufenkji, Nathalie, & Elimelech, M. (2004). Deviation from the classical colloid filtration theory in the presence of repulsive DLVO interactions. *Langmuir : the ACS journal of surfaces and colloids*, *20*(25), 10818–28. doi:10.1021/la0486638

Tufenkji, Nathalie, & Elimelech, M. (2005). Breakdown of colloid filtration theory: role of the secondary energy minimum and surface charge heterogeneities. *Langmuir*, *21*(3), 841–852. doi:10.1021/la050850y

Walker, S., Redman, J., & Elimelech, M. (2004). Role of Cell Surface Lipopolysaccharides in Escherichia coli K12 adhesion and transport. *Langmuir : the ACS journal of surfaces and colloids*, *20*(18), 7736–46. doi:10.1021/la049511f

Walker, S., Redman, J., & Elimelech, M. (2005). Influence of growth phase on bacterial deposition: interaction mechanisms in packed-bed column and radial stagnation point flow systems. *Environmental science & technology*, *39*(17), 6405–11. Retrieved from http://www.ncbi.nlm.nih.gov/pubmed/16190193

Windbacher, T. (2010). *Engineering Gate Stacks for Field-Effect Transistors*. Vienna University of Technology.

Yates, M. V, Gerba, C. P., & Kelley, L. M. (1985). Virus persistence in groundwater. *Applied and environmental microbiology*, *49*(4), 778–81. Retrieved from http://www.pubmedcentral.nih.gov/articlerender.fcgi?artid=238444&tool=pmcentrez&rendertype=abstract

Zheng, Q, Dickson, S. E., & Guo, Y. (2009). Differential transport and dispersion of colloids relative to solutes in single fractures. *Journal of colloid and interface science*, *339*(1), 140–51. doi:10.1016/j.jcis.2009.07.002

Zheng, Q., Dickson, S. E., & Guo, Y. (2008). On the appropriate "equivalent aperture" for the description of solute transport in single fractures: Laboratory-scale experiments. *Water Resources Research*, *44*(4), 1–9. doi:10.1029/2007WR005970

Zheng, Q., Dickson, S., & Guo, Y. (2009). Influence of aperture field heterogeneity and anisotropy on dispersion regimes and dispersivity in single fractures. *Journal of Geophysical Research*, *114*(B3), 1–12. doi:10.1029/2007JB005161

Zheng, Qinghuai. (2008). *Effect of Aperture Variability, Specific Discharge and Ionic Strength on Colloid Transport in Single Fractures*. McMaster University.

Zimmerman, R. W., & Bodvarsson, G. S. (1996). Hydraulic Conductivity of Rock Fractures. *Transport in Porous Media*, *23*(1), 1–30.

Zvikelsky, O., & Weisbrod, N. (2006). Impact of particle size on colloid transport in discrete fractures. *Water Resources Research*, *42*(12), 1–12. doi:10.1029/2006WR004873

Appendix A – Materials and Methods

Bacteria, bacteriophage and microsphere transport and retention through single, saturated fractures were investigated in this work by creating effluent concentration profiles in a laboratory setting. This work explored the relative importance of electrostatics on the adhesion and retardation mechanisms for particle transport through fractured material. Further, the transport characteristics of microspheres relative to similar sized biological material were investigated in order to evaluate their use as a surrogate material. These conclusions were drawn for two fractures of similar material, but highly different aperture field characteristics, allowing for further comments on the relative importance of hydraulics on colloid retention. All experiments were conducted at identical specific discharge rates of 15 m/day to facilitate comparisons between experiments.

This section seeks to clarify extensive amounts of information used to set up the experiment, gather the data, analyze the data and quantify confidence around the data sets.

Fracture source and induction

Rock samples were obtained from the DoLime Quarry in Guelph, Ontario. Guelph is a town located in the middle of Southwestern Ontario, as shown in Figure 12. The majority of water obtained for public consumption in the city of Guelph is pumped from fractured bedrock aquifers. Fractures utilized for this work were obtained from the Guelph rock formation, characterized by a relatively higher permeability and lighter hue (Burke, 2012).

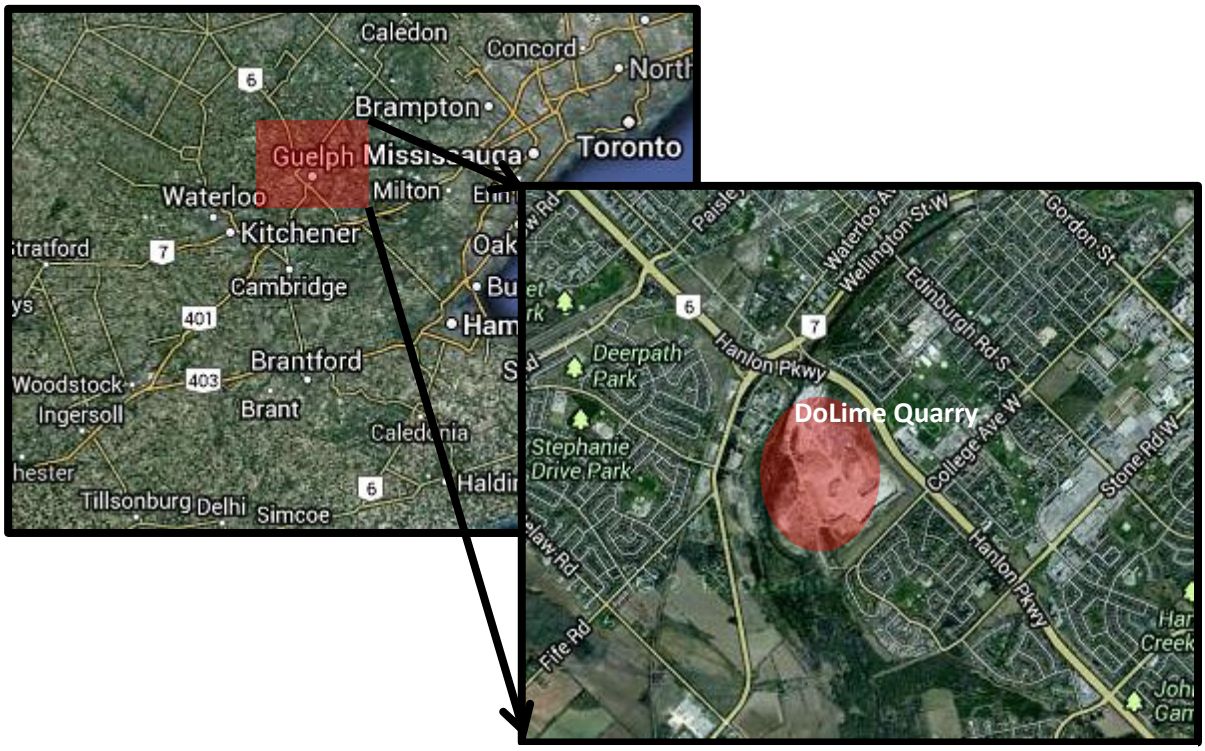

Figure 12 - Detail regarding the location of Guelph and the DoLime quarry.

Solid samples were roughly cut from this quarry and taken back to the Environmental Systems Laboratory at McMaster University where the faces of the samples were recut using a diamond blade (Schutten, 2012). Longitudinal reinforcements were then added prior to a uniaxial force being applied along an identified plane of weakness. This method is similar to the process by which natural fractures would be created in nature to relieve stress from tension or compression (Schutten, 2012). This quality was desired, to ensure that fractures were representative of natural fractures. Further, based on the reinforcement applied, it is hypothesized that secondary fractures induced within this system were minimal. While the technique used to create the two fractures was identical, major differences between the fractures were observed. Mainly, Fracture 2 was subject to the formation of additional chips of rock, while Fracture 1 was a relatively clean break. While it was attempted to place the chips back in the correct place within the fracture field, not all chips could be recovered. This created interesting aperture differences between the fractures. Overall, the fracture dimensions are as follows:

Table 6 - Rock fracture characteristics

	Length	Width
Fracture 1	0.41 m	0.31 m
Fracture 2	0.49 m	0.30 m

Final Experimental Set Up and Saturation

A picture of the final experimental set up is shown as Figure 13 below. On both the upstream and downstream sides of the fracture, a plastic end cap was attached to the fracture creating a flow cell. Material within this cell was circulated, allowing for each to be modeled as a continuously stirred tank reactor (CSTR). Based on this assumption, the precise inlet and outlet concentrations of material from the fracture can be calculated.

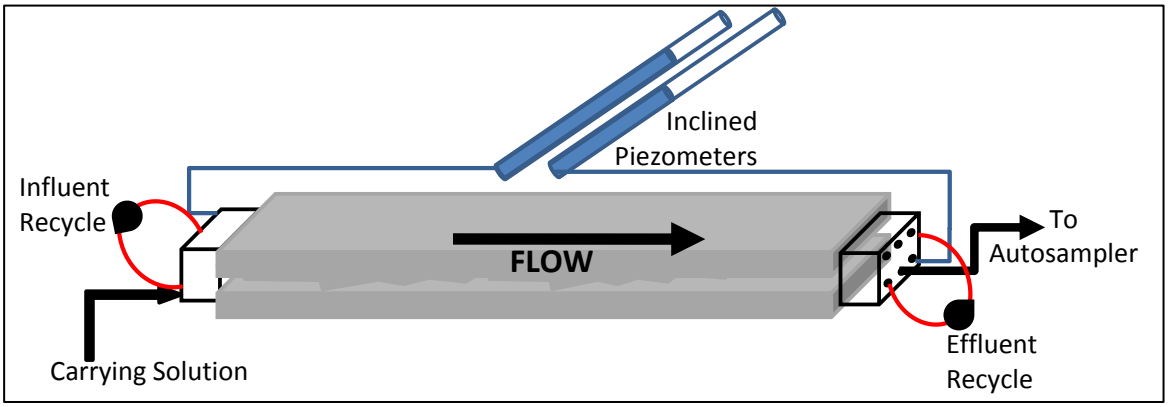

Figure 13 - Final Experimental Set Up

Although the upstream and downstream faces were cut with a saw, they were not square. As a result, the flow cell was not flush with the surface of the rock fracture. In order to bridge this gap, a polyurethane O ring was custom cut and placed in the gap. Flow cells were secured tightly against the O ring using plastic strapping, allowing each flow cell and O ring to remain in place on the fracture without the aid of an adhesive. The gap between the flow cell and fracture was made water tight using a silicone sealant. This experimental designed ensured that the silicone was not responsible for holding the load of the fracture cells. Further, the O ring helped to bridge the gap between the flow cell and fracture, giving the silicone additional material to seal to.

Into each flow cell, six 1/8" NPT holes were cut and threaded. On both upstream and downstream flow cells, a circulation system was constructed. In order to facilitate this, nylon bore-through Swagelock® fittings were utilized to allow for the use of a perforated tube within

the flow cell, promoting more thorough mixing. The perforated tube was connected to opposite corners on the flow cell, as shown in Figure 14 below, again to promote mixing within the cell. Outside the flow cell, a mixture of tubing was used as required. More durable Norprene tubing (McMaster-Carr, 1/16" ID, 3/16" OD) was used in the peristaltic pump head. Within each circulation system, a custom glass sampling piece, modified from a glass sampling vial, was included. Each vial was capped with a plastic lid and a Teflon sided septa, protecting the fluid inside the system while allowing for the withdrawal of samples using a syringe. Connecting the sampling vial, Norprene tubing and perforated mixing tube was Tygon PVC microbial resistant tubing (McMaster-Carr, B-44-4X), sized as appropriate to fit between the different sections. It is important that this tubing was microbial *resistant*, helping to reduce the bacterial growth within the tube while not killing microbes that are within the system (important since this work considers both *E. coli* and MS2 transport).

The inclined piezometer was connected to the remaining hole in the bottom corner, marked in red on Figure 14 below. The inclined piezometers were constructed out of glass tubing, and held at a known angle to calculate the vertical head drop across the fracture. For the inlet flow cells, the bottom middle hole (marked in green) was utilized as the influent point, and was connected to the source liquid. For outlet flow cells, the top corner opposite of the recirculation system was connected to the autosampler and is marked blue. Not all holes were used continuously for all experiments. When not in use, holes were sealed. Tubing used between the outlet flow cell and the autosampler was a very small diameter (1/16" I.D.) to reduce the time and mixing that will occur in the tube.

To ensure complete saturation of the rock fracture, the fracture and both flow cells were first flooded with carbon dioxide gas. This gas is more soluble in water and ensures the removal of as many air bubbles as possible. The fracture would then be flushed for at least 12 hours to ensure the dissolution of as much carbon dioxide as possible. Careful inspection for leak detection was carried out throughout the saturation process. Water to be flushed through the fracture was kept in 20 L carboys upstream of each fracture. PBS of varying concentrations was primarily used as the carrying fluid to introduce the desired conductivity and to maintain fluid pH. Use of pure MilliQ (18.2 mΩ resistance) water was avoided as much as possible to prevent the dissolution of rock into the stream.

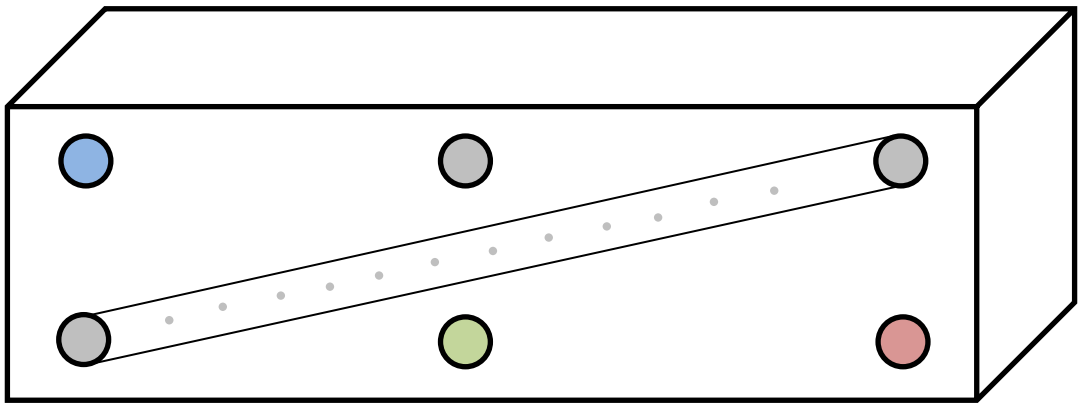

Figure 14 - Example diagram of perforated mixing tube within each flow cell

Hydraulic Experiments

Hydraulic experiments worked to measure the pressure differential across the fracture length in order to generate estimates for the average aperture across the flow field. Generally, the flow rate through each fracture was altered and the corresponding pressure differential was measured. At relatively laminar flow, it is expected that this relationship is linear. Flow rate was measured by collecting a given volume of fluid from the rock effluent over a period of time. From (35), it is seen that the hydraulic aperture is dependent on several additional measurements, all of which have associated measurement error. Table 7 below shows the variable and quantification of measurement error.

$$b_c = \left(\frac{12\mu QL}{\rho g W \Delta h}\right)^{\frac{1}{3}} \tag{35}$$

Table 7 - Summary of Hydraulic Test Measurement Errors

Variable	Measurement Technique	Error
Length of fracture	-Ruler with cm markings	±0.001 m
Width of Fracture	-Ruler with cm markings	±0.001 m
Flow Rate	-Graduated cylinder with 0.1mL accuracy	±1.0x10^{-7} m^3/(time of collection)
Vertical Head Differential	-Either a transparent fixed measuring tape or callipers depending on the fracture	±0.0005 m

To determine the overall error associated with these measurements, propagation of error was used. Error for (35) was computed in two steps. Consider first the intermediate function *F* as (36). Using propagation of error techniques, error for this function, *ΔF*, can be calculated as (37) (Figliola & Beasley, 2006).

$$F = \frac{12\mu QL}{\rho g W \Delta h} \tag{36}$$

$$\Delta F = \sqrt{\left(\frac{\partial F}{\partial Q}\cdot \Delta Q\right)^2 + \left(\frac{\partial F}{\partial L}\cdot \Delta L\right)^2 + \left(\frac{\partial F}{\partial W}\cdot \Delta W\right)^2 + \left(\frac{\partial F}{\partial h}\cdot \Delta h\right)^2} \tag{37}$$

As a secondary step, propagated error from the exponential term can then be calculated as (38) (Figliola & Beasley, 2006).

$$\Delta b_c = \left|\frac{1}{3}\right| \frac{\Delta F}{|F|} |b_c| \tag{38}$$

Using these calculation techniques, adequate estimations of error were generated for the cubic law aperture.

Conservative Tracer Experiments

Tracer experiments were carried out to determine the parameter τ which is the average residence time within the fracture. Bromide was used as a tracer because of its inert properties and ease with which its concentration can be found. Tracer experiments were only began once the background concentration of bromide was negligible. To commence a tracer test, the fluid driving pumps were first turned off. 0.75 mL of 10 g/L sodium bromide solution was injected into the front flow cell and allowed to mix thoroughly. The driving peristaltic pumps were then turned on again and time was started. For all conservative tracer experiments, the carrying fluid was a dilute phosphate buffer solution (PBS) in order to maintain solution pH and reduce the dissolution of rock. Bromide was selected as the tracer because it is expected to undergo limited reactions and adhesions with the experimental set up, and therefore lead to a high recovery approaching 100%.

Concentration of bromide in effluent samples was completed using high performance liquid chromatography (HPLC). For this work specifically, an anion column from Hamilton Company (PRP-X110) was used to separate bromide ions. A calibration curve was used to determine concentration of samples. Samples were run in triplicate through the HPLC to determine the variance of the readings. Tracer experiments were carried out at three specific discharge rates of 5 m/day, 15 m/day and 30 m/day to see the effect of flow rate on tracer flow. The slower two experiments were completed in duplicate to test the repeatability of the experimental method and experimental set up.

From effluent concentration curves, the following analysis was utilized to find the average residence time and percent recovery. It is assumed that flow cells on the inlet and outlet of the fracture act as perfectly mixed continuous stirred tank reactors (CSTRs), so the exact inlet and out concentrations of the rock fracture can be found. The influent concentration of material into the fracture can be approximated by considering a mass balance on the inlet CSTR, and is simplified into (39) below.

$$C_{in}(t) = C_o e^{\left(\frac{-vt}{V}\right)} \tag{39}$$

Where v is the volumetric flow rate, t is time, V is the volume of the inlet CSTR and C_o is the initial concentration of tracer in the inlet CSTR. For purposes of this research, initial concentration was often calculated based on the known amount of tracer added and the inlet cell volume.

Similar to this idea, the effluent concentration from the fracture can be calculated, again considering a mass balance around the effluent CSTR. This equation is shown below as (40). Here, variables are as presented in (39). Additionally, Q is the volumetric flow rate and C_{meas} is the measured concentration from the sample obtained. The rate of concentration change is approximated from the measured effluent concentration.

$$C_{out}(t) = \left(\frac{V}{Q}\right)\left(\frac{dC}{dt}\right) + C_{meas} \tag{40}$$

Therefore, the concentration of tracer into and out of the actual fracture can be calculated. As explained by Fahim & Wakao (1982), this data can be used to calculate the mean tracer time

within the fracture. The relationship between the influent concentration (C_{in}) and effluent concentration (C_{out}) can be defined by the transfer function *F(s)* shown below in (41) below. Equation (42) correlates this transfer function to major transport parameters τ (mean residence time) and N_D (dispersion number).

$$F(s) = \frac{\int_0^\infty C_{out} e^{-st} dt}{\int_0^\infty C_{in} e^{-st} dt} \tag{41}$$

$$F(s) = \exp\left(\frac{1}{2N_D}\left(1 - (1 + 4N_D \tau s)^{\frac{1}{2}}\right)\right) \tag{42}$$

While this paper introduces several methods of data interpretation, the weighted moment method was utilized in this research to calculate the mean residence time of tracer within the fracture. From Fahim and Wakao, the nth weighted moment and central moment can be calculated according to (43) and (44) below. Note that these moments can be calculated separately for the inlet and outlet concentration curves.

$$m_n = \frac{\int_0^\infty C t^n e^{(-st)} dt}{\int_0^\infty C dt} \tag{43}$$

$$\mu_n = \frac{\int_0^\infty C \left(t - \frac{m_1}{m_0}\right)^n e^{(-st)} dt}{\int_0^\infty C dt} \tag{44}$$

In these equations, integrals can be approximated numerically using calculated effluent concentration curves. From the weighted moment analysis, the following relationships with the transfer function and transport variables can be made.

$$\frac{m_0^{in}}{m_0^{out}} = F(s) \tag{45}$$

$$\frac{m_1^{out}}{m_0^{out}} - \frac{m_1^{in}}{m_0^{in}} = -\frac{F'(s)}{F(s)} = \bar{\tau}(1 + 4N_D \tau s)^{\left(-\frac{1}{2}\right)} \tag{46}$$

$$\frac{\mu_2^{out}}{m_0^{out}} - \frac{\mu_2^{in}}{m_0^{in}} = \frac{d}{ds}\left(\frac{F'(s)}{F(s)}\right) = 2\tau^2 N_D (1 + 4N_D \tau s)^{\left(-\frac{3}{2}\right)} \tag{47}$$

To use the weighted moment method, a series of equations and unknowns must be solved. One parameter, *s*, is a fitting parameter to provide a more adequate solution. However, the problem becomes: which value of *s* to use to properly fit the equations. The other transport parameters can be found by solving a system of equations (either (42) and (46) or (46) and (47)), but the correct value of *s* to use directly depends on the order of weighted moment calculated. Fahim & Wakao (1982) present several empirical methods used to estimate this parameter. However, due to the uncertainty of effluent concentration, the estimated *s* parameter is widely variable and therefore drastically affects the calculation of the other parameters. Other literature sources suggest that the optimum value of *s* to use occurs when the variability in parameter estimation is minimized (Anderssen & White, 1971). Fahim and Wakao explore this idea by selecting different values for the weighting parameter and observing the effect on the calculated parameters. They noticed that there was an area of low sensitivity, where changes in the weighting parameter did not alter final parameter estimations by a significant amount, likely indicated the most appropriate parameter values. Trial of multiple *s* parameter values was carried out to find the area of lowest sensitivity, which was then assumed to be the most correct solution of equations. Confidence around the calculated τ was up to the judgement of the researcher, and led to the confidence interval around the τ term. Each sample was processed in triplicate in the HPLC. High and low estimates for the bromide concentration were created by adding or subtracting three standard deviations of the sample measurement. The data was then reanalyzed considering these two new curves to generate a confidence interval around the percent recovery.

Bacteriophage MS2 Experiments

As previously discussed, bacteriophage MS2 is a non-pathogenic virus that will exclusively infect host *E. coli* bacteria. It was selected for this work due to its size similarity to other pathogenic viruses, to understand how very small biological particulate material will transport. MS2 is an icosahedral virus with a diameter of approximately 20-25 nm.

MS2 bacteriophage used in this work was obtained from Maria Mesquita at the University of Waterloo. Freezer stock of MS2 was created from the initial sample using a liquid propagation method. Host *E. coli* bacteria were grown into the exponential growth phase, then inoculated with the MS2 sample. This inoculated sample was incubated at 37°C for a further

eight hours while mixing. After this infection period approximately 100 µL of chloroform was added and the mixture was allowed to sit at room temperature overnight. On the subsequent day, the mixture was centrifuged at 6000 g for ten minutes. The resulting supernatant was filtered through a 0.2µm filter. Care was taken during centrifugation to ensure the speed was sufficient to pelletize host cell material while leaving the desired virus in solution. Filtering the supernatant was completed to further remove cell debris and purify MS2 stock. Further purification through PEG precipitation is possible, but was not deemed necessary for this work. Additionally, there exists a solid propagation method whereby phage are grown on plates, scraped off the surface and purified. Samples were mixed with about 15% glycerol by volume, dispensed into 1.5 mL cryogenic vials and kept at -80°C until use.

Prior to an MS2 test, one vial was removed from the freezer, thawed and serially diluted for enumeration purposes. For all MS2 experiments, 1 mL of the (-3) dilution was injected into the upstream flow cell and thoroughly mixed prior to starting the test. Samples were collected at pre-determined intervals and plated according to the process outlined in Figure 15 below. Recipes for all solutions used are presented later in this appendix.

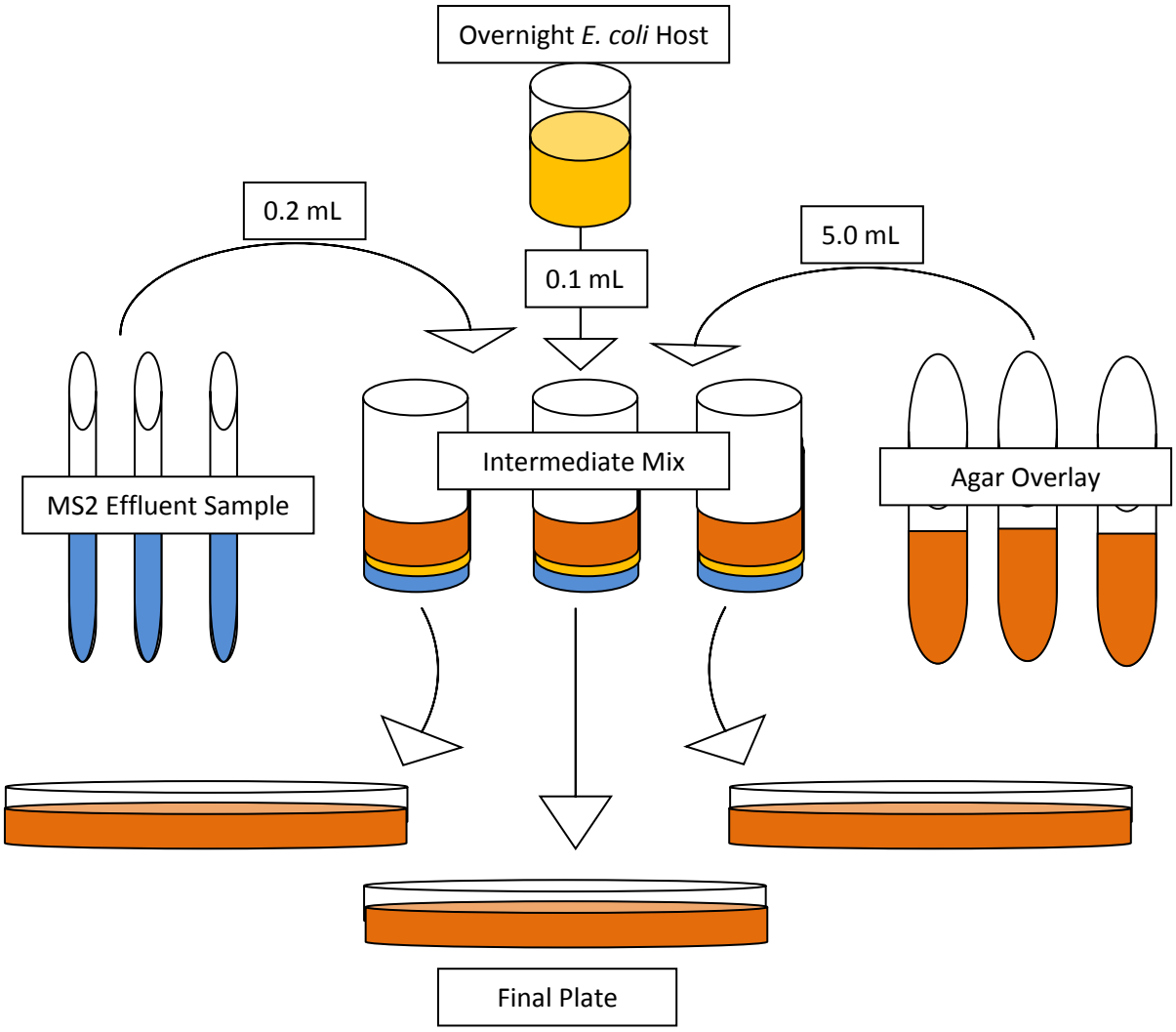

Figure 15 - Diagram showing the MS2 enumeration plating process

The MS2 enumeration process is diagrammed in the figure above. The required equipment for enumerations is as follows:

- Final plates with 1.5% TSA agar base
- 0.75% TSA agar overlay tubes, dispensed into 5 mL/tube
- Calcium chloride solution, 0.2µm filter sterilized
- Sufficient intermediate mix containers, previously autoclaved

First, agar was inoculated with *E. coli* host on the day prior to plating. In the morning, the overnight host was placed on ice to maintain its growth state. Into a secondary mixing vessel,

0.2 mL of sample was added to 0.1 mL of *E. coli* host and 0.1 mL of a calcium chloride solution, which promotes infection. This mixture was allowed to sit for three minutes while infection took place. Soft agar overlay (0.7% TSA) was liquefied and kept in a water bath at 52°C. 5 mL of this agar overlay was then added to the intermediate mixing vessel, swirled and quickly poured over the 1.5% TSA agar on the final plate. This mixture is allowed to harden before the plate is inverted and incubated at 37°C for 12-20 hours. Plates that were incubated for only 12 hours had a reduced chance of drying out while having no effect on the final plaque count. Effluent samples were obtained for 96 hours after commencing the test. Over the first 48 hours, ionic strength of the transport solution was kept constant at approximately 8.7 mM. After this time, the ionic strength of the solution was significantly reduced to approximately 0.58 mM. This allowed for the evaluation of the effect of ionic strength on the transport characteristics, effectively estimating the importance of electrostatics and the applicability of the DLVO theory to biological contaminants.

Each sample was plated in triplicate to understand more about the error associated with the plating process. Methodology as described by Emelko et al., (2010a, 2010b) was utilized to calculate the actual MS2 concentration within each sample. This methodology was used for all biological particulate material, and is described in another section of this appendix. Using the logarithm from Emelko et al., (2010b), high and low estimates of MS2 concentration were developed. Analogous to previous analyses, these high and low estimations were used to develop confidence intervals around the percent recovery and mean residence time calculations.

E. coli Bacteria Experiments

E. coli RS2GFP was selected for use in these experiments. It is a non-pathogenic strain of *E. coli* and is resistant to kanamycin and rifampicin antibiotics. This particular strain has been modified to carry a green fluorescent protein, allowing the bacteria to be visually tracked given the correct lighting conditions. Therefore, it is expected to be representative of pathogenic *E. coli* transport, such as O157:H7, the strain responsible for the Walkerton outbreak. Further, use of antibiotics in all agars reduces contamination potential, increasing the confidence in the results. Generally, *E. coli* is a gram-negative, rod shaped bacteria. This particular strain was obtained from Dr. Larry Halverson from the Department of Agriculture and Biosystems

Engineering at Iowa State University via the laboratory of Dr. Emelko in the Department of Civil Engineering at the University of Waterloo.

Fractures were prepped for *E. coli* experiments by first ensuring the background concentration of *E. coli* was negligible. Ionic strength within the fractures was required to be approximately 8.7 mM and stable prior to test commencement. Several conductivity measurements were taken prior to test start to ensure this took place.

It was desirable that the *E. coli* be in its exponential growth phase at the beginning of the test to ensure consistency between experiments. On the day prior to an *E. coli* test, a culture of *E. coli* was incubated overnight. 0.5 mL of the overnight culture was transferred to a day culture, where the optical density was monitored closely. *E. coli* reaches its exponential growth phase when the optical density is measured to be between 0.5-0.8 at a 520nm wavelength. The *E. coli* sample is then washed to remove the agar food source and maintain the bacterial concentration. This is completed by centrifuging the entire sample at 5000 RPM for 10 minutes. The broth is then decanted off the top, and a phosphate buffer solution (PBS) is poured into the centrifuge tube. The *E. coli* is re-suspended in the tube through agitation, and the centrifuge process is repeated to ensure thorough washing. *E. coli* titres could be concentrated or diluted slightly during the washing process as well.

E. coli experiments were run at specific discharge rates of 15 m/day. The washed *E. coli* stock was enumerated to determine the initial concentration of bacteria. A sample of this was kept at room temperature beside the fractures and continually enumerated to measure the bacterial decay over the course of the test. Samples were collected using a fractionator, and enumerated as close to the draw time as possible. Using the washed *E. coli* stock as the model decay curve, samples were adjusted to determine their actual concentration at the time of drawing.

E. coli enumeration was completed using a plating technique. This process is shown in Figure 16. Simply, 0.1 mL of sample is added to the top of a plate that has been pre poured with LB Agar. The sample is spread around with a sterile stick and allowed to dry before inverting and incubating for 12-24 hours. All samples were plated in triplicate to help quantify uncertainty in the measurements.

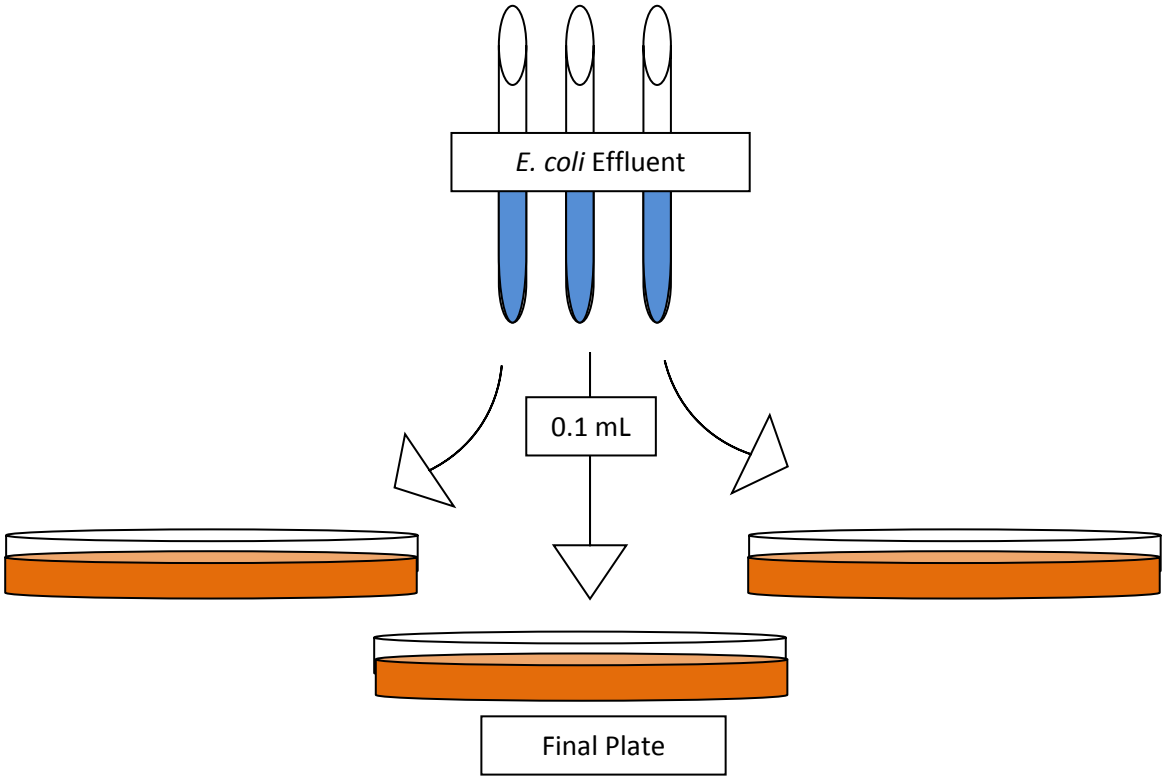

Figure 16 - Plating procedure for *E. coli* samples

Microbial Test Uncertainty

Uncertainty associated with enumeration of microbial samples has been described and qualified in a series of papers by Emelko et al., (2010a, 2010b). In these papers, it is claimed that microbial data are uncertain because of five major sources of error, which are detailed below.

Representative Sampling Error – Variations within the source concentration will lead to enumeration differences. Within the construct of this experiment, this error source is not expected to be relevant, since discrete samples are collected from the source, and the source, the effluent mixing cell, is assumed to be a CSTR. Further, changes in the source concentration are expected and quantification of these changes is a major experimental goal. In the methodology presented by Emelko et al., (2010a, 2010b), this error source is not explicitly considered.

Random Sampling Error – Repeat samples from the same source contain different numbers of particles. In this work, two separate samples are grabbed; one using the autosampler from the

effluent of the rock fracture, and another smaller one from this sample to plate in the enumeration process. This second sample is subject to random sampling error, and samples of identical volumes may contain a different number of particles.

Analytical Error – The processing methodology used results in incomplete recovery of particles from the sample. Both microbial experiments rely on a plating process for enumeration. Analytical error would occur if this process is not 100% efficient, and reliably results in the loss of some particles in the sample. With respect to bacteriophage, another way to describe this error is to consider the efficiency of plating (EOP). The EOP considers the ratio of particle concentration as determined by plating vs. the true particle concentration as determined by another, typically more rigorous method (Adams, 1959). It has been shown that the EOP can directly relate to the bacteriophage and host strains used (Lennox, 1955). Similarly, error inherent within the bacteria plating process may lead to lower recovery than the true concentration. For both *E. coli* and MS2 experiments, the exact efficiency was not known. Therefore, efficiencies were estimated based on reasonable assumptions. Since this error is applied to all processed samples, it is not expected to have an impact in the observed results; rather it ensures that all sources of error are considered in the enumeration process.

Non Constant Analytical Recovery – Two identically processed samples result in different enumerations. As an example, bacteriophage plating procedure uses an interim mixing container, while bacteria plating uses a spreading stick. Both may be sources for particle adhesion, resulting in reduced enumeration counts. However, the effect on final counts is unpredictable and therefore termed non constant. There may be several sources of non-constant analytical error within each plating procedure.

Counting Error – Repeated counts of a processed sample result in different enumerations. As stated previously, plates with counts between 10 and 300 are targeted to reduce the observed error. However, occasionally even plates well within these limits produce areas that are difficult to decipher, and may result in the counting error described here.

Bayesian Statistics

Generally, Emelko et al., (2010a) suggest that final enumeration uncertainty can be estimated if the errors above can be approximated. They use Bayesian statistics to estimate the

posterior probability function. Simply, to determine the posterior probability, you need a prior distribution (in this case, the results from plating) and the odds of making the given observation. Therefore, several assumptions about the nature of the errors presented above must be made in order to estimate the final uncertainty. Emelko et al., (2010a, 2010b) present two methods for quantifying uncertainty, the Beta-Poisson and the Negative binomial. The differences between these stem from the methods they use to quantify error. For the purpose of this work, the Beta-Poisson was used to estimate uncertainty. This method assumes that error imparted from random sampling error follows a Poisson distribution, and analytical error is described by a binomial distribution. Finally, recovery from the plating process used follows a beta distribution and encompasses all the non-constant analytical error.

The posterior distribution describing the true effluent concentrations is not analytically calculable due to the complex relationships used to describe error within the measurements. Further, it is both time and money consuming to create a large number of enumeration plates. Therefore, Gibbs sampling can be used to approximate the posterior distribution based on limited initial observations. To implement this model, an estimation of the recovery parameters is required. Further, a number of 'burn in' iterations are preformed to ensure the recorded concentrations are sufficiently near the expected concentration. Generally, this Gibbs sampling methodology will provide a pseudo-random sampling of the posterior distribution expected given the initial plating observations. This methodology is only pseudo-random because each iteration depends on previous estimations for each parameter. Additional information regarding the development of the Gibbs sampling methodology can be found in Emelko et al., (2010a, 2010b). Code used to implement the methodology in MatLab can be found below.

Gibbs Sampling Procedure – MatLab Code

```
reps=3;          %is the total number of times enumeration was repeated
enum=[1:reps];   %dimensions vector with correct number of entries
tcount=[1:reps];%vector where 'true counts' will be placed based on
observations and stats
pconst=[1:reps];%recovery constant
svol=[1:reps];   %measure of the volumes tested for each sample
z=1;             %simple count variable
y=1;             %simple count variable
trial=1;

enum=[24,33,42];    %defines enumeration vector, as counted on plate
svol=[0.1,0.1,0.1]; %volume of sample in mL
```

```
dil=10^-0;

numburn = 50;   %number of 'burn in' iterations
numsave = 5000;  %number of true iterations that will be analyzed

tempconc = 0;       %temporary true concentration value for transitional
use
trueconc = [1:numsave];%Markov chain of posterior concentration values
concvol =1; %product of concentration and volume sum

%Constants A and B are ideally found from a controlled recovery study.
For example, it is assumed a recovery of 90% was observed from a true
titre of 5e12. This would correspond to a count of 500 at a -10 dilution
A=mean(enum);
B=mean(enum)/9;

Sumtcount=0;    %Total of true counts
Sumpconst=0;    %Total of recovery constants
Sumvol=0;       %Total of sample volumes

%Initial estimation for concentration
for z = 1:reps
    tcount(z)=round((enum(z)*(A+B)/A));
    Sumtcount=Sumtcount+tcount(z);
    Sumvol=Sumvol+svol(z);
end

Lamda=[1:reps];

%Gibbs Sampling
for trial = 1:(numburn+numsave)
    concvol=gamrnd(Sumtcount+1,1);
    tempconc=concvol/Sumvol;
    if trial>numburn
       trueconc(trial-numburn)=(tempconc/dil);
    elseif trial<=numburn
        burnconc(trial)=tempconc;  %elseif put in to examine NaN error
    end
    Sumtcount=0;
    y=1;
    for y=1:reps
        pconst(y)= betarnd((enum(y)+A), (tcount(y)-enum(y)+B));
        Lamda(y)=tempconc*svol(y)*(1-pconst(y));
        tcount(y)=poissrnd(Lamda(y))+enum(y);
        Sumtcount=Sumtcount+tcount(y);
    end
    y=1;
end

avg=mean(trueconc);
stdev=std(trueconc);
```

```
sorttc=sort(trueconc);
subtot=0;
i=0.025*numsave;
for i=0.025*numsave:0.975*numsave;
    subtot=subtot+sorttc(i);
    i=i+1;
end

high=sorttc(0.975*numsave);
low=sorttc(0.025*numsave);

g=(min(trueconc):(max(trueconc)-min(trueconc))/80:max(trueconc));
figure
hist(trueconc,g)
hold on
plot([avg,avg],[0,200],'red')
hold on
plot([low,low],[0,200],'red')
hold on
plot([high,high],[0,200],'red')

figure
plot(trueconc)
hold on
plot([0,numsave],[avg,avg],'red');
hold on
plot([0,numsave],[high,high],'red');
hold on
plot([0,numsave],[low,low],'red');

credinterval=subtot/sum(trueconc)
Summary=[avg,high,low]
```

List of Experimental Solutions Used

Broth and Agar Solutions for Bacteriophage MS2

0.7% Trypticase Soy Agar (TSA) – For top layer bacteriophage enumeration

Into 1L of deionized (DI) water, add:

- 30 g Trypticase Soy Broth (TSB)
- 5 g Salt
- 7 g Bacto Agar

While mixing, dispense into 5mL of the solution into vials. Autoclave the vials at 121°C for 15 minutes and store at 4°C until use.

1.5% TSA – For bottom layer bacteriophage enumeration

Into 1L of DI water, add:

- 40 g TSA

The entire solution was autoclaved at 121°C for 15 minutes. Once the solution had cooled to a temperature where it could be handled, approximately 15 mL of agar was poured into the dish. The dish was gently swirled to cover the entire bottom of the dish, and set aside to let cool. Work was completed in a sterile environment to avoid contamination. Solidified plates are inverted and stored at 4°C until use.

TSB – To facilitate *E. coli* host growth

Into 1L of DI water, add:

- 25 g TSB

Let the solution cool and store at 4°C.

Glucose/Calcium Chloride Solution – This solution is used as an additive during bacteriophage enumeration to encourage infection of the bacterial host. Into 20 mL of DI, add:

- 1 g D-Glucose
- 0.3 g $CaCl_2 \cdot H_20$

Mix the solution thoroughly. Sterilize the solution by filtering through a 0.22 µm filter and store at room temperature.

Phosphate Buffer Solution (PBS)

Three different PBS solutions were utilized throughout the completion of this work. Firstly, 'regular strength' PBS (rsPBS) was used for all dilutions that were required as part of the enumeration of biological material. To complete the actual test, carrying solution similar to actual groundwater conditions was desirable. Saleh & Kim, (2008) have documented the ionic strength of typical groundwater to be approximately 2-10 mM of monovalent ions and 0.1-2 mM of divalent ions. Groundwater strength PBS (gwPBS) was created with these recommendations. Finally, a goal of this work was to evaluate the electrostatic interactions between the particles and the fracture surface. In order to accomplish this, the ionic strength of the carrying solution was significantly reduced after 2 days of running the experiments. This reduced conductivity (rcPBS) was used to alter the expected electrostatic interactions between the particle and fracture surface while still maintaining biological viability and a pH buffer.

rsPBS

Into 1L of DI, add:

- 8 g of NaCl
- 0.2 g of KCl
- 0.12 g KH_2PO_4
- 1.67 g $Na_2HPO_4 \cdot 7H_2O$

Dispense the desired amount into test tubes, cap loosely and autoclave at 121°C for 15 minutes. Store the test tubes at room temperature until use. pH of the PBS solution should be 7.5.

gwPBS

Into 1L of DI, add:

- 0.4 g NaCl
- 0.016 g KCl
- 0.012 g KH_2PO_4
- 0.167 g $Na_2HPO_4 \cdot 7H_2O$

Disinfection procedure is analogous to that listed above. The expected ionic strength of this solution is 8.7 mM. Effluent conductivity was regularly measured slightly higher than this, likely due to the impacts from the dolomite fracture.

rcPBS

Into 1L of DI, add:

- 0.01 g of KH_2PO_4
- 0.05 g $Na_2HPO_4 \cdot 7H_2O$

Disinfection procedure is analogous to above. The expected ionic strength of this solution is 0.58 mM. Effluent conductivity was regularly measured slightly higher than this, likely due to the impacts from the dolomite fracture.

Expected ionic strengths were calculated using an iterative process. It is known that the concentration of phosphates (and therefore of sodium and potassium ions) would be in equilibrium and depend on the pH of the solution. Relevant equations were derived from the Henderson-Hasselbach equation (48) to find the phosphate concentrations. The ionic strength (I), (49), was then calculated as a summation of all expected ions within the solution. Dissociation constants, dependent on the ionic strength within solution, were then modified according to the Debye-Hückel relationship, (50), and the iteration was repeated. Relevant equations are presented below (Windbacher, 2010).

$$pH = pKa + \left(\frac{[acid]}{[base]}\right) \tag{48}$$

$$I = 0.5 * \sum (c_i)({z_i}^2) \tag{49}$$

$$pK'a = pKa + (2\varepsilon_a - 1)\left(\frac{A\sqrt{I}}{1+\sqrt{I}} - 0.1I\right) \tag{50}$$

Solutions for *E. coli* rs2GFP

Antibiotics:

Kanamycin

Into 100 mL of DI, add:

- 1 g Kanamycin

Sterilize this solution by filtering through a 0.22 µm filter. Store the solution in plastic bottles at -80°C.

Rifampicin

Into 100 mL of methanol:

- 0.1 g Rifampicin

Store the solution in an amber bottle at 4°C.

Broth

The broth is used to cultivate *E. coli* for host propagation or overnight growth. Into 1L of DI, add:

- 10 g HiVeg Hydrolysate (HIMEDIA RM030v-500G)
- 10 g NaCl
- 5 g Yeast Extract (Bacto BD 212750)

Mix thoroughly and autoclave for 15 minutes at 121°C. After the solution has cooled, add:

- 10 mL Kanamycin
- 10 mL Rifampicin

Store the solution at 4°C until use.

Agar:

Agar is used as the bottom layer on each plate. It is the media upon which samples containing *E. coli* will be added and incubated overnight. Into 1L of DI, add:

- 15 g Agar (Bishop AGR003.500)
- 10 g HiVeg Hydrolysate (HIMEDIA RM030v-500G)
- 10 g NaCl
- 5 g Yeast Extract (Bacto BD 212750)

Mix thoroughly and autoclave for 15 minutes at 121°C. Allow the solution to cool and add:

- 10 mL Kanamycin

- 10 mL Rifampicin

Mix through the antibiotics, pour the agar into the plates and allow the agar to solidify. Care should be taken prior to antibiotic addition, as the agar must be cool enough to maintain antibiotic integrity, but warm enough to allow for plate pouring before it all hardens. After solidification, plates are inverted and stored at 4°C until use.

Solutions for HPLC

For all HPLC work, a Hamilton a PRP-X110 column was used to separate anions from the given sample. All samples were first filtered through a 0.22µm filter to protect the column and guard. Further, it was recognized that both eluent and regenerant concentrations could be varied to produce the desired outcome. For example, if peaks were desired to come out of the column faster or tighter, eluent concentration or flow rate could be increased. Regenerant flow rate and or concentration would then need to be adjusted to reflect the required balance. Below shows one potential operating condition that was utilized for this work.

Eluent (1.5x Strength)

- 1.34 g NaOH
- 3.82 g Hydroxybenzoic Acid (HBA)
- 115 mL Methanol

Appendix B – Additional Results

Bromide Tracer Test Results

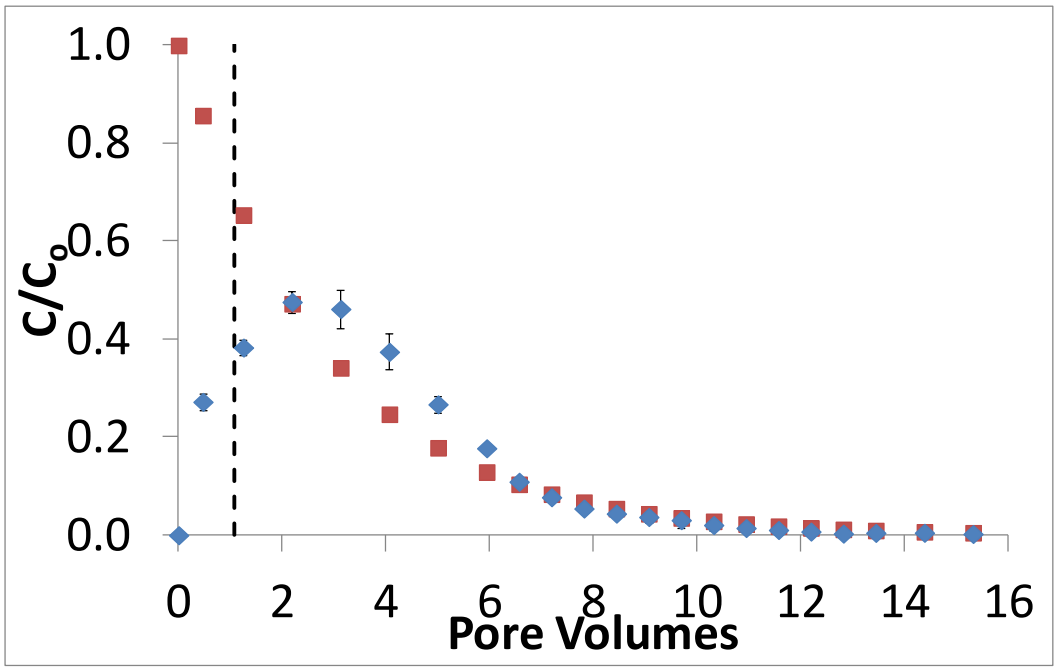

Figure 17 - Effluent concentration curve, Fracture 1 at 30 m/day
Figure shows inlet (■), and effluent (◆) results. Average residence time is shown by the hatched line.

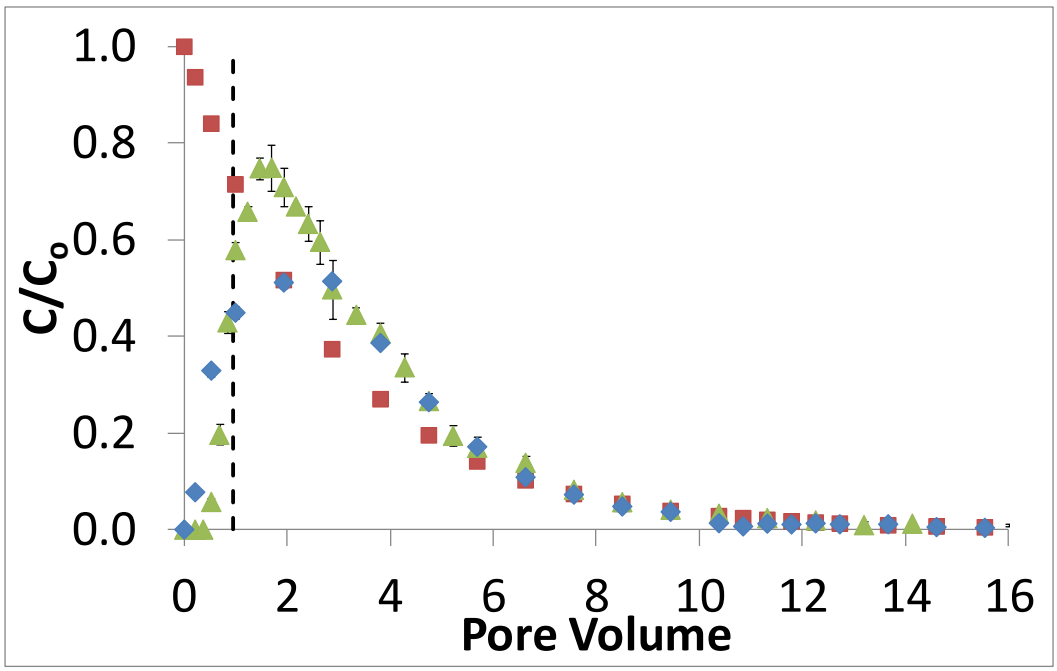

Figure 18 - Effluent concentration curve, Fracture 1, 5 m/day
Figure shows inlet (■), test 1 (◆) and test 2 (▲) results. Average residence time is shown by the hatched line.

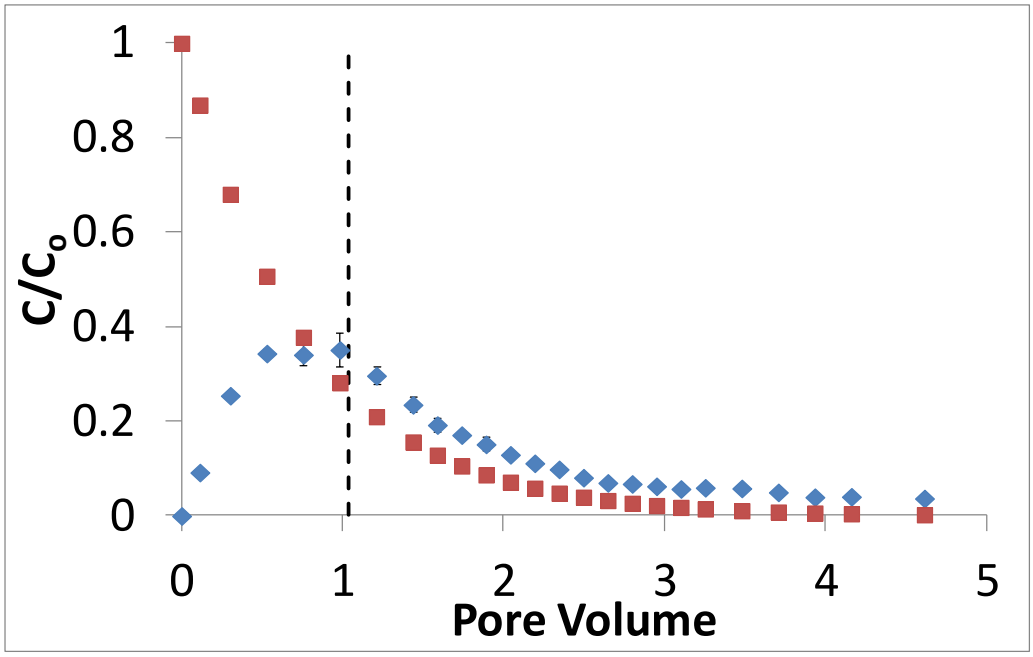

Figure 19 - Effluent concentration curve, Fracture 2, 30 m/day
Figure shows inlet (■), and effluent (◆) results. Average residence time is shown by the hatched line.

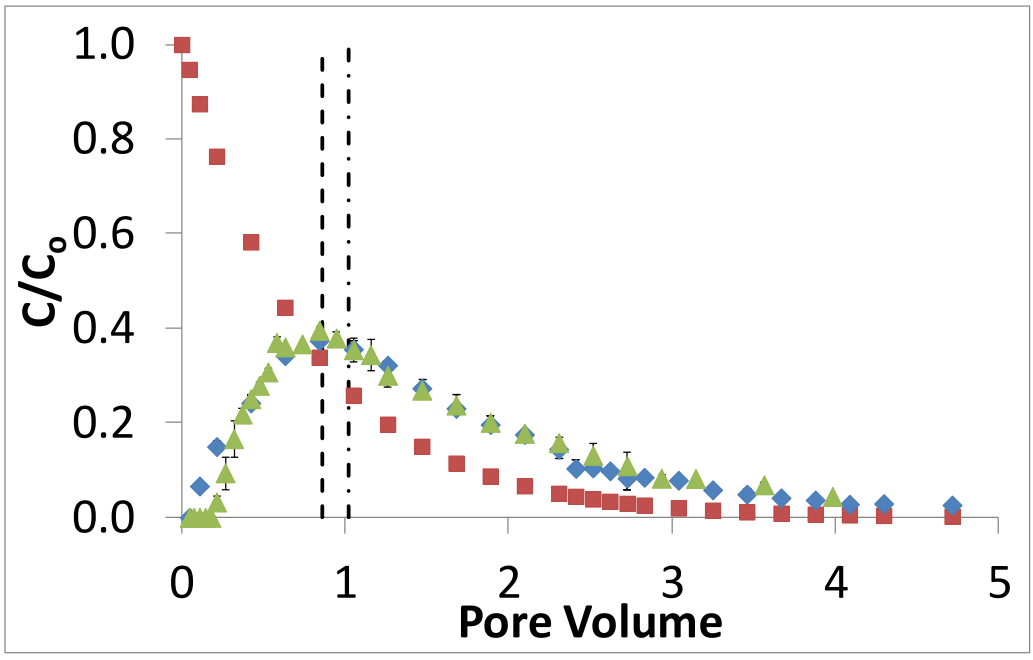

Figure 20 - Effluent concentration curve, Fracture 2, 5 m/day
Figure shows inlet (■), test 1 (◆) and test 2 (▲) results. Average residence time is shown by the hatched line.